UNCLASSIFIED

AD NUMBER
AD321352
CLASSIFICATION CHANGES
TO: unclassified
FROM: confidential
LIMITATION CHANGES
TO: Approved for public release, distribution unlimited
FROM: Distribution authorized to U.S. Gov't. agencies and their contractors; Administrative/Operational Use; NOV 1960. Other requests shall be referred to Office of Naval Research, Arlington, VA 22203.
AUTHORITY
ONR ltr, 28 Jul 1977; ONR ltr, 28 Jul 1977

THIS PAGE IS UNCLASSIFIED

THIS REPORT HAS BEEN DELIMITED
AND CLEARED FOR PUBLIC RELEASE
UNDER DOD DIRECTIVE 5200.20 AND
NO RESTRICTIONS ARE IMPOSED UPON
ITS USE AND DISCLOSURE.

DISTRIBUTION STATEMENT A

APPROVED FOR PUBLIC RELEASE;
DISTRIBUTION UNLIMITED.

Best
Available
Copy

321 352

Reproduced
by the

S TECHNICAL INFORMATION AGENCY
INGTON HALL STATION
LINGTON 12, VIRGINIA

NOTICE: When government or other drawings, specifications or other data are used for any purpose other than in connection with a definitely related government procurement operation, the U. S. Government thereby incurs no responsibility, nor any obligation whatsoever; and the fact that the Government may have formulated, furnished, or in any way supplied the said drawings, specifications, or other data is not to be regarded by implication or otherwise as in any manner licensing the holder or any other person or corporation, or conveying any rights or permission to manufacture, use or sell any patented invention that may in any way be related thereto.

CATALOGED BY ASTIA
AS AD No. 324 352

MASSACHUSETTS INSTITUTE OF TECHNOLOGY
NAVAL SUPERSONIC LABORATORY

Technical Report 430

(Unclassified Title)
ROCKET THRUST CONTROL
BY GAS INJECTION

by

John J. Blaszak
and
Fred E. Fahrenholz

November 1960

XEROX

628.3

ASTIA
JAN 30 1951
D

CONFIDENTIAL

Massachusetts Institute of Technology
Naval Supersonic Laboratory

Technical Report 430

(Unclassified Title)
ROCKET THRUST CONTROL BY GAS INJECTION

by

John J. Blaszak
and
Fred E. Fahrenholz

November 1960

This report contains x
and 77 pages. Copy No. 21
of 160 copies.

NSL Log 3784

CONFIDENTIAL

CONFIDENTIAL

FOREWORD

The research described in this report was sponsored in whole or in part by the Office of Naval Research under Contract Nonr 1841(61) which has been monitored by Lt. Cmdr. F. T. Hemmler, Lt. Cmdr. W. L. Miller and Mr. J. R. Patton, Jr.

Reproduction in whole or in part of material contained in this report is permitted for any purpose of the United States Government.

CONFIDENTIAL

ABSTRACT

A study is being conducted at the Naval Supersonic Laboratory to determine the feasibility of a new method of rocket thrust control. The method is one in which the injection of a secondary flow throttles the primary or main nozzle flow.

The initial phase of the work centered around the use of a low pressure-ratio nozzle exhausting to atmosphere. A variety of secondary injection configurations were ed. All of these were located in the throat region of the main nozzle. Asymmetric (axially) as well as symmetric configurations were investigated.

Results obtained thus far indicate that significant flow throttling can be achieved through secondary injection. Nozzle thrust is directly proportional to total flow and total flow is approximately linearly related to secondary injection rate. Performance is a strong function of injection angle but insensitive to injection orifice arrangement or asymmetry A relatively simple analytical model was devised which agrees with the flow throttling data.

TABLE OF CONTENTS

TABLE OF CONTENTS (Concluded)

LIST OF ILLUSTRATIONS

LIST OF ILLUSTRATIONS

LIST OF ILLUSTRATIONS (Concluded)

LIST OF SYMBOLS

A_n	Nozzle exit area
A_s	Secondary injection slot area
A_{1_s}	Secondary flow area where local Mach number is M_{1_s}
A_{2_s}	Secondary flow area at Station 2
A_{*_s}	Secondary injection orifice area (where local Mach number is unity)
b_1	Slot width
b_2	Width of secondary flow at Station 2 (see sketches on pages 13 and 15)
C_p	Specific heat at constant pressure
C_v	Specific heat at constant volume
g	Gravitational constant
M	Mach number
M_{1_s}	Secondary Mach number as flow enters nozzle
p	Pressure
p_{atm}	Atmospheric pressure (~ 14.7 psia)
p_0	Primary stagnation pressure
p_{0_s}	Secondary stagnation pressure
R	Gas constant
R	Radius of primary flow (see sketches on pages 13 and 15)
T	Temperature
T	Thrust
T_0	Primary stagnation temperature
T_0	Thrust with unrestricted primary flow ($w_s = 0$)

LIST OF SYMBOLS (Concluded)

V_p	Velocity corresponding to isentropic expansion from p_0 to atmosphere
V_s	Velocity corresponding to isentropic expansion from p_{0_s} to atmosphere
w_p	Primary flow
w_{p_c}	Unrestricted primary flow ($w_s = 0$)
w_s	Secondary flow
β	Circumferential angle over which injection takes place
γ	Ratio of specific heats $\left(\frac{C_p}{C_v}\right)$
ρ	Density
ρ_0	Primary stagnation density
ϕ	Injection angle (see sketch on page 13)

Subscripts

$_1$, $_2$	Flow stations in primary flow, see sketches on pages 13 and 15
$_{1_s}$, $_{2_s}$	Flow stations in secondary flow, see sketches on pages 13 and 15
*	Value at sonic speed, M = 1

SECTION I

INTRODUCTION

As modern rocket engines move toward the million pound thrust range, the problem of thrust vector control becomes increasingly important. Gimbal systems have become enormous and, as yet, good methods of engine throttling are virtually nonexistent. The need for more efficient systems is apparent.

The Naval Supersonic Laboratory (NSL), encouraged by the NACA work reported in Ref. 1, proposed to the Office of Naval Research (ONR) to undertake a program of investigation of a new method of rocket thrust control. In December 1958, ONR support was furnished under Contract Nonr 1841(61) to perform a Phase I feasibility study of the problem.

The method of thrust control under study here involves the use of a secondary flow which effectively throttles the main nozzle flow. It was felt that symmetric injection for thrust modulation and asymmetric injection for vector control should prove to be efficient.

The Phase I results are summarized in detail in the present report. These results have been promising enough to warrant further study of the parameters affecting thrust control.

SECTION II

EARLY WORK

A. UNITED AIRCRAFT CORPORATION

Control of the thrust vector of a nozzle by means of fluid injection was first investigated by the Research Department of the United Aircraft Corporation (UAC). The important features of this investigation are discussed briefly in this section.

The method, in general terms, involves the injection of a secondary gas into a main nozzle to alter the main flow. In the UAC studies (Ref. 2), the secondary gas was injected into the supersonic (divergent) portion of a convergent-divergent nozzle for the purpose of changing the thrust vector direction. As expected, the resultant generation of shock waves altered the pressure field in such a way as to add to the reaction force of the secondary jet. The thrust vector was thus changed and control was achieved by varying the secondary flow.

The UAC experiments were concerned with conical nozzles and several injection configurations. The conical divergent sections of all of the nozzles had a semi-vertex angle of 15°. Nozzle exit-to-throat area ratios ranged from 8.0 to 25.0. Sonic and supersonic injection port geometries were tested at various locations in the primary nozzles. Almost all of the tests involved the use of single injection ports; only one test had two ports, located 90° apart. In all cases, the injection port axis was perpendicular to the nozzle wall.

The primary nozzle throat diameter was 0.85 inches while the stagnation pressure and temperature were 320 psia and 100°F, respectively. Air was used as the working fluid in both the primary and secondary flows. The secondary flow rate was varied to a maximum of 10 percent of the primary flow rate, both flows were measured with flowmeters. The thrust and side force were measured directly by means of strain gage techniques.

The UAC measurements indicated that side force is directly proportional to secondary flow rate. In addition, this result was found to be independent of the primary nozzle area ratio and pressure ratio as well as the injection port location (whose range was well into the supersonic portion of the nozzle). In particular, the side force generated is approximately 1.4 times the calculated reaction force of the secondary jet. The results for supersonic injection ports showed sensitivity to nozzle contour in that performance improves with shaping for parallel flow at the exit. However, supersonic injection, per se, does not increase the side force induced in the primary nozzle. The configuration with two injection ports showed that, based on equal total secondary flow rates, the side force generated in a plane mid-way between the ports was less than that for a single injection port.

A similarity parameter was also developed which correlated a limited amount of previously obtained data. That data was from both cold and hot gas tests made by UAC and the Naval Air Rocket Test Station, respectively. The parameter was derived from a simple analytical approach which approximated the physical situation. A ratio of side force to thrust was developed of the form

$$\frac{\text{Side Force}}{\text{Thrust}} = \left\{ \begin{array}{c} \text{function of gas properties and primary} \\ \text{and secondary flow Mach numbers} \end{array} \right\}$$

$$\times \frac{\text{Secondary Flow Rate}}{\text{Primary Flow Rate}} \times \sqrt{\frac{\text{Secondary Flow Stagnation Temp}}{\text{Primary Flow Stagnation Temp}}}$$

where the expression in brackets is only functionally defined. The hot and cold gas data was found to vary in a linear fashion with the flow ratio times the square root of the temperature ratio Thus the expression in brackets may be represented by an empirical constant.

In summary, it may be said that the UAC work initiated the concept of fluid injection as a means of nozzle thrust control. The tests conducted by UAC were by no means an exhaustive study of the method In fact, the results cited above show that an increase of side force of

only 40 percent is realized over that which would be obtained with the secondary flow not directed into the primary nozzle. Nevertheless, the number and possible variation of the parameters involved indicated that there were areas yet to be explored.

B. NACA

The NACA also investigated the secondary injection method of flow control. The NACA experiments, reported in Ref. 1, concerned symmetric injection for flow throttling as well as asymmetric injection for flow deflection. This program was designed to evaluate gas injection as a means of controlling the exhaust area of a jet engine nozzle. The following is a brief discussion of the NACA study.

1. Model and Instrumentation

The NACA investigation concerned a convergent main (primary) nozzle into which secondary gas was injected from a circumferential slot at the nozzle exit (which is also the minimum section). The primary nozzle was a conical one with a semi-vertex angle of 8° and an exit diameter of 4.0 inches. The injection slot directed the secondary gas perpendicular to the primary nozzle axis. The slot width was varied such that the ratio of slot area to primary nozzle exit area ranged from 0.018 to 0.468. Asymmetric injection for primary flow deflection was achieved by blocking a portion of the circumference of the slot. Symmetric injection means that the entire slot circumference was filled with secondary gas.

The primary nozzle exhausted to atmosphere and was operated at pressure ratios of 1.6, 2.0, 2.4, and 2.8. The ratio of secondary stagnation pressure to atmospheric pressure was varied between 2.0 and 7.7. Air was the working fluid in the primary and secondary flows, both of which were measured with standard ASME orifices. The stagnation temperature of both streams was approximately 530°R. The nozzle assembly was held by a suspension system in which thrust and side force were measured with force cells.

2. Test Results

a. Symmetric Injection

The results obtained with symmetric injection showed that the reduction in primary flow, which is related to thrust, varies almost in direct proportion to secondary flow rate. Some typical measurements have been plotted in Fig. 1 where primary flow is plotted against secondary flow. The basic significance of the results shown is that the reduction in primary flow is greater than the corresponding injected secondary flow. In addition, as the pressure ratio of the primary nozzle is increased, a given primary flow reduction requires more secondary injection. However, the rate of increase of secondary flow required is smaller than the corresponding rate of increase of primary pressure ratio. This is reasonable once the primary pressure ratio exceeds the sonic value (about 1.88). Thereafter the flow behavior should be sensitive to the secondary-to-primary stagnation pressure ratio rather than the overall pressure ratio of the primary nozzle.

Although the data shown in Fig. 1 corresponds to a slot-to-exit area ratio of 0.033, it is typical of the other slot widths. That is, the data is similar regarding the remarks just above. There is, however, a variation in performance with slot width. This variation is illustrated by the data shown in Fig. 2 which also corresponds to symmetric injection. The increase in primary flow reduction (at a given w_s/w_{p_0}) with decreases in slot width, shown for a primary pressure ratio of 2, is typical. This effect may be due to the fact that potential secondary momentum is not available at the low secondary pressure ratios which accompany large slot widths and high flow rates.

A simple analytical model is discussed in Ref. 1 which was used to correlate some of the symmetric injection data. It is similar to one that was developed earlier by Martin (Ref. 3) which is discussed in detail in the next section. It is an empirical method in which an experimentally determined factor correlates the data but does not prove the model.

A parameter was devised for use as a measure of the efficiency

of the nozzle in generating thrust. It is called the thrust ratio and defined as

$$\frac{\text{Thrust}}{\frac{w_p}{g} V_p + \frac{w_s}{g} V_s}$$

where the velocities V_p and V_s are the flow speeds attained by a perfect gas in an isentropic flow expansion from the appropriate stagnation pressures to atmospheric pressure. For symmetric injection it was found that the thrust ratio was between 0.94 and 0.98 in nearly all cases. Thus, not only is the nozzle thrust proportional to total flow but it appears that the throttling process is an efficient one.

b. Asymmetric Injection

Nozzle performance was also measured, as mentioned previously, with asymmetric secondary injection. Some of the results in these tests have been plotted in Fig. 3. This figure shows the flow throttling achieved with asymmetric injection. Despite the large difference in A_s/A_n from that of Figs. 1 and 2, flow throttling performance is similar to that with much smaller A_s/A_n. The effect of primary pressure ratio is the same as that shown in Fig. 1, and this is also true at ratios other than those shown in Fig. 3. In addition, the effect of A_s/A_n is the same as that shown in Fig. 2, and this also pertains to other primary pressure ratios. Some effect of the circumferential angle of injection is observable in that a slightly greater primary flow reduction (at a given w_s/w_{p_0}) occurs with an angle of 45 as opposed to 90 degrees.

A parameter called the side force ratio was devised for use in comparing the performance of the asymmetric injection configurations. The side force ratio is merely the side force divided by the same denominator as that in the thrust ratio. The total measured side force ratio for these same configurations is plotted against secondary flow in Fig. 4. The effect of primary pressure ratio on the side force ratio is similar to that at pressure ratios not shown. This effect is seen to be one which decreases the side force (at a given w_s/w_{p_0}) as the primary pressure ratio

is increased. This decrease has two sources, both of which are related to the significant flow throttling shown in Fig. 3. First, the reduced effective flow area (in injection zone), inherent with throttling, increases the static pressure (as velocity decreases) on the walls upstream of the injection slot. This increased static pressure decreases the momentum of the secondary flow. Second, and more important, as throttling increases with secondary flow, the pressure distribution (which produces side force) on the walls upstream of the injection slot becomes less asymmetrical.

Also shown in Fig. 4 are the effects of slot width (A_s/A_n) and circumferential injection angle (β). Side force decreases (at a given w_s/w_{p_0}) as slot width is increased, at a constant β of 90°. This is the result, as in the previous case with symmetric injection, of decreased secondary momentum associated with lower secondary pressure ratios. A smaller effect on side force is noted for the circumferential injection angle β. Side force increases (at a given w_s/w_{p_0}) as β decreases from 90° to 45° with the effect being more pronounced at the higher primary pressure ratio. At pressure ratios higher than those shown, the effect is like that at a primary pressure ratio of 2. It should be mentioned, however, that a decrease in β must increase side force since secondary injection is then more closely aligned with the side force direction. In view of this fact, the conclusions just made should be regarded as being somewhat tenuous.

The merit of asymmetric injection was partly judged in Ref. 1 by a comparison to the theoretical performance of a similar configuration operated external to the primary nozzle. Although enumerated only in a few cases, results were apparently similar to those of UAC. In particular, the gain (over external operation performance) in side force varied between 0 and 100 percent. However, gains higher than about 50 percent were realized only at very small flows (less than w_s/w_{p_0} of 0.04).

3. Summary

In summary, it may be said that the NACA work reported in Ref. 1

constituted a significant extension of the UAC effort. articular importance was the use of symmetric injection for flow ...ottling. In this connection, results with a convergent nozzle sho.. .hat performance is a strong function of secondary flow rate and also varies ... intly with injection slot width and primary pressure ratio.

In the case of asymmetric injection, flow throttling was found to be a similar function of the same variables as those of importance with symmetric injection. A significant amplification in side force attends asymmetric injection over a range of secondary flow rates. According to Ref. 1, however, the associated primary flow throttling would limit application to the jet engine nozzle problem.

Unfortunately, the lack of a clear specification of experimental error injects some uncertainty into the results. Nevertheless, the significant trends are no doubt dependable.

SECTION III

THEORY OF THE AERODYNAMICALLY VARIABLE NOZZLE

A flow analysis has been devised which is substantiated by the NSL (Phase I) experimental data. The NSL water table studies and the work reported in Ref. 3 contributed significantly to the development of the NSL theoretical model. The first part of this section presents the theory developed by Martin in Ref. 3. The remainder of this section briefly describes a water table study and develops, in detail, the NSL theory.

A. MARTIN THEORY

The problem of secondary injection into a main stream is considered by Martin in Ref. 3. Secondary injection is viewed as a possible method of obtaining a nozzle with a variable throat. It is pointed out, as in the NACA report (Ref. 1), that such a nozzle would be of use in controlling the performance of a jet engine at different operating conditions.

Martin developed two theoretical models for the flow which occurs with secondary injection. The first is based on the assumption that the injected gas mixes completely with the main stream. The second one assumes that the jet flow will be separated from the main stream by means of a vortex sheet. Although these models are treated individually, it should be noted that this procedure is regarded as a simplification necessary to generate an amenable analytical problem. It is most likely, as Martin points out, that in the real case both effects will be present.

Although the two theoretical flow configurations are discussed separately below, certain simplifying assumptions are common to both. The most basic one is that the flow is one-dimensional. In addition, the primary and secondary fluids are assumed to be perfect gases whose flow is isentropic. A further assumption is that the local injection pressure and temperature (hence density) are equal to the stagnation values in the main stream. It was not suggested by Martin that these

conditions are actually satisfied but rather that their use leads to an approximately correct choice of dependence of variables.

The assumption of isentropic, perfect gas flow immediately relates certain problem variables in a unique fashion. The equation of state for a perfect gas,

$$p = \rho R T \tag{1}$$

relates the pressure, density, and temperature at any point in the flow. As shown in Ref. 4, the energy equation may be written in the following appropriate form:

$$\frac{T}{T_0} = \left[1 + \frac{\gamma - 1}{2} M^2 \right]^{-1} \tag{2}$$

In addition, the energy equation is useful in obtaining the following one-dimensional isentropic flow relations:

$$\frac{p}{p_0} = \left[1 + \frac{\gamma - 1}{2} M^2 \right]^{-\frac{\gamma}{\gamma - 1}} \tag{3}$$

$$\frac{\rho}{\rho_0} = \left[1 + \frac{\gamma - 1}{2} M^2 \right]^{-\frac{1}{\gamma - 1}} \tag{4}$$

All of the above equations apply throughout the flow in both theoretical models.

1. Mixing Process Case

In the mixing process case the secondary gas mixes with the primary flow to produce a combined stream. The sketch on the following page shows the important features of the flow configuration. The secondary flow enters the nozzle (radius R_1) through a slot (width b_1) and is directed at an angle ϕ with respect to the nozzle axis.* The primary

*The Mach number of the secondary flow as it enters the nozzle is M_{1_S} — other properties at this location are identified by the same subscript notation.

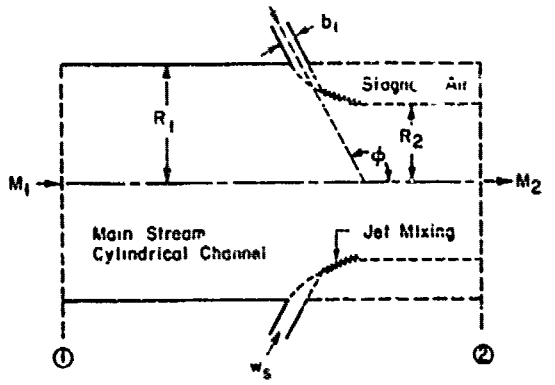

and secondary streams mix to form a final stream tube of radius R_2. The primary stream flows uniformly at Mach number M_1 at station 1 while a uniform combined stream flows past station 2 at Mach number M_2.

The equations of continuity and momentum are then applied to the flow and, in particular, are evaluated at stations 1 and 2. The appropriate form of the equation of continuity is

$$\rho_2 R_2^2 M_2 \left[\gamma R T_2\right]^{\frac{1}{2}} = \rho_1 R_1^2 M_1 \left[\gamma R T_1\right]^{\frac{1}{2}} + 2 R_1 b_1 \rho_0 M_{1_s} \left[\gamma R T_{1_s}\right]^{\frac{1}{2}} \quad (5)$$

in which, as mentioned above, the local injection density is taken as the stagnation value in the primary stream. The continuity equation may be rewritten as

$$\frac{\rho_2}{\rho_0}\left[\frac{R_2}{R_1}\right]^2 M_2 \left[\frac{T_2}{T_0}\right]^{\frac{1}{2}} = \frac{\rho_1}{\rho_0} M_1 \left[\frac{T_1}{T_0}\right]^{\frac{1}{2}} + 2\frac{b_1}{R_1} M_{1_s} \left[\frac{T_{1_s}}{T_{0_s}}\right]^{\frac{1}{2}} \left[\frac{T_{0_s}}{T_0}\right]^{\frac{1}{2}} \quad (6)$$

where the primary and secondary fluids are the same gas. The assumption that $T_{1_s} = T_0$ simplifies Eq. (6) since the temperature ratios cancel one another in the second term on the right hand side of the equation.

The equation of momentum is applied in the form

$$\rho_1 R_1^2 + \rho_1 R_1^2 M_1^2 \gamma R \left[\frac{T_1}{T_0}\right] T_0 - 2 b_1 R_1 \rho_0 M_{1_s}^2 \gamma R \left[\frac{T_{1_s}}{T_{0_s}}\right] T_{0_s} \cos \phi$$

$$= \rho_2 R_1^2 + \rho_2 R_2^2 M_2^2 \gamma R \left[\frac{T_2}{T_0}\right] T_0 \qquad (7)$$

which, like Eq. (5), is the general representation. As above, with the primary and secondary streams being the same gas, the momentum equation simplifies to

$$\frac{p_1}{p_0} + \gamma M_1^2 \left[\frac{p_1}{p_0}\right] - 2\frac{b_1}{R_1} \gamma M_{1_s}^2 \left[\frac{T_{1_s}}{T_{0_s}}\right] \left[\frac{T_{0_s}}{T_0}\right] \cos \phi$$

$$= \frac{p_2}{p_0} + \gamma M_2^2 \left[\frac{R_2}{R_1}\right]^2 \frac{p_2}{p_0} \qquad (8)$$

This equation, however, has the additional assumption that the average stagnation density of the combined stream is equal to the initial primary stagnation density. Martin shows that this introduces a negligible error. As in Eq. (6), the temperature ratios cancel in the third term on the left hand side of Eq. (8).

When certain final assumptions are made the continuity and momentum equations (6 and 8) yield a solution to the problem. The geometry is specified by the assumption of values for the parameters b_1/R_1 and ϕ while the particular gas employed designates γ. The final assumptions necessary are an initial secondary Mach number M_{1_s} and the overall pressure ratio p_2/p_0 (also implies an M_2). In addition, the pressure, density, and temperature ratios in Eqs. (6) and (8) are functions of Mach number according to Eqs. (2), (3), and (4). Thus, Eqs. (6) and (8) are a pair of simultaneous equations with unknowns $[R_2/R_1]^2$ and M_1.

2. Vortex Sheet Case

The basic assumption in the vortex sheet case is that the primary and secondary streams do not mix. The flow configuration is shown in the sketch below.

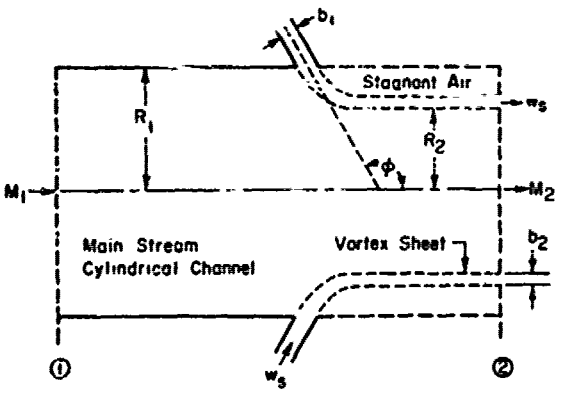

The secondary flow enters the nozzle in the same manner as that in the mixing process case. In the vortex sheet case, however, the primary and secondary flows are two distinct streams at station 2. At this station, the primary stream has a radius R_2 while the surrounding cylinder of secondary flow has a thickness b_2. In addition to the corresponding Mach numbers in the mixing process case, there is a secondary M_{2_s} at station 2.

There are two equations of continuity for the vortex sheet case. The appropriate one for the primary flow is

$$\rho_2 R_2^2 M_2 \left[\gamma R T_2\right]^{\frac{1}{2}} = \rho_1 R_1^2 M_1 \left[\gamma R T_1\right]^{\frac{1}{2}} \qquad (9)$$

which may be manipulated to the form

$$\frac{\rho_2}{\rho_0}\left[\frac{R_2}{R_1}\right]^2 M_2 \left[\frac{T_2}{T_0}\right]^{\frac{1}{2}} = \frac{\rho_1}{\rho_0} M_1 \left[\frac{T_1}{T_0}\right]^{\frac{1}{2}} \qquad (10)$$

The continuity equation for the secondary flow is given by

$$\rho_{2_s} R_2 b_2 M_{2_s} \left[\gamma R T_{2_s}\right]^{\frac{1}{2}} = \rho_0 R_1 b_1 M_{1_s} \left[\gamma R T_{1_s}\right]^{\frac{1}{2}} \qquad (11)$$

where, as in the mixing process case, the local injection density is taken as the stagnation value in the primary stream. Equation (11) has the form of Eq. (10) when rewritten as

$$\frac{\rho_{2_s}}{\rho_0}\left[\frac{R_2\ b_2}{R_1\ b_1}\right] M_{2_s}\left[\frac{T_{2_s}}{T_{0_s}}\right]^{\frac{1}{2}} = M_{1_s}\left[\frac{T_{1_s}}{T_{0_s}}\right]^{\frac{1}{2}} \qquad (12)$$

It should be pointed out that the secondary continuity equation contains the approximation that the cross sectional area of the cylindrical secondary flow is $2\pi R_2 b_2$. This is a good approximation as long as $b_2/R_2 << 1$ which would be the case if the secondary flow rate is small compared to the primary one.

The momentum equation for the vortex sheet case is

$$p_1 R_1^2 + \rho_1 M_1^2 \gamma R\left[\frac{T_1}{T_0}\right] T_0 R_1^2 - 2 b_1 R_1 \rho_0 M_{1_s}^2 \gamma R\left[\frac{T_{1_s}}{T_{0_s}}\right] T_{0_s} \cos\phi$$

$$= p_2 R_1^2 + \rho_2 M_2^2 \gamma R\left[\frac{T_2}{T_0}\right] T_0 R_2^2$$

$$+ 2 b_2 R_2 \rho_{2_s} M_{2_s}^2 \gamma R\left[\frac{T_{2_s}}{T_{0_s}}\right] T_{0_s} \qquad (13)$$

This equation may be simplified by manipulation and substitution of Eq. (12), which results in the form

$$\frac{p_1}{p_0} + \gamma M_1^2\left[\frac{p_1}{p_0}\right] - 2\frac{b_1}{R_1}\gamma M_{1_s}^2\left[\frac{T_{1_s}}{T_{0_s}}\right]\left[\frac{T_{0_s}}{T_0}\right]\cos\phi$$

$$= \frac{p_2}{p_0} + \gamma M_2^2\left[\frac{p_2}{p_0}\right]\left[\frac{R_2}{R_1}\right]^2 + 2\frac{b_1}{R_1} M_{1_s} M_{2_s}\gamma\left[\frac{T_{0_s}}{T_{1_s}}\right]^{\frac{1}{2}}\left[\frac{T_{2_s}}{T_{0_s}}\right]^{\frac{1}{2}} \qquad (14)$$

In this equation, as in Eq. (8), the temperature ratios cancel one another in the third term on the left hand side of the equation.

The continuity and momentum equations yield a problem solution, as in the mixing process case, dependent upon certain final assumptions. These necessary assumptions are those of the mixing process case plus an additional one. The additional assumption necessary is a specification for M_{2_S}. However, Martin assumes that p_2 is equal to p_{2_S} which implies a value for M_{2_S}, as follows. The assumed M_{1_S} implies a p_{1_S}/p_{0_S} and

$$\frac{p_{1_S}}{p_{0_S}} = \frac{p_0}{p_{0_S}}$$

Also, as stated above

$$\frac{p_2}{p_0} = \frac{p_{2_S}}{p_0}$$

and thus

$$\frac{p_0}{p_{0_S}} \times \frac{p_{2_S}}{p_0} = \frac{p_{2_S}}{p_{0_S}}$$

which implies the value of M_{2_S} (by Eq. 3).

The pressure, density, and temperature ratios in Eqs. (10) and (14) are, as mentioned previously, functions of Mach number. The determination of M_{2_S} according to the procedure above then makes Eqs. (10) and (14) a pair of simultaneous equations with unknowns $\left[R_2/R_1\right]^2$ and M_1.

3. Theoretical Results and Experiment

The calculations carried out for the two Martin flow models are presented in the following paragraphs. It should be noted that the methods as presented in the preceding sections employ a different notation than that used by Martin.

a. Secondary Flow

In the mixing process and the vortex sheet case, the secondary flow rate is governed by the same equation. In non-dimensional

form, the secondary flow may be written as

$$\frac{w_s}{w_{p_0}} = \frac{2\pi R_1 b_1 \rho_0 M_{1_s} \left[\gamma R T_{1_s}\right]^{\frac{1}{2}}}{\pi R_1^2 \rho_2 M_2 \left[\frac{T_2}{T_0}\right]^{\frac{1}{2}} \left[\gamma R T_0\right]^{\frac{1}{2}}} \qquad (15)$$

By the assumptions that were mentioned previously, Eq. (15) simplifies to

$$\frac{w_s}{w_{p_0}} = \frac{2\left[\frac{b_1}{R_1}\right] M_{1_s}}{\left[\frac{\rho_2}{\rho_0}\right] M_2 \left[\frac{T_2}{T_0}\right]^{\frac{1}{2}}} \qquad (16)$$

Equation (16) shows that the secondary flow ratio varies directly with M_{1_s}.

b. Flow Throttling

The work reported by Martin included an experiment, and the data obtained was compared to the results predicted by the two analytical models. The calculations carried out by the NSL were for the same conditions as this Martin case. The NSL method and results (similar to Martin's results) are presented below along with the appropriate comparison to the data.

It was mentioned in the previous sections that a problem solution requires certain final assumptions. In accordance with Ref. 3, the geometry was specified by $b_1/R_1 = 0.02$ and $\phi = 70°$. Air was the working fluid ($\gamma = 1.4$) and the overall primary pressure ratio ($p_2/p_0 = 0.5283$) was such that $M_2 = 1$. The related assumptions yield a relationship for secondary flow ratio (from Eq. 16) which is illustrated in Fig. 5.

The final equations for both flow models were solved by a graphical technique. As indicated in the previous sections, a problem solution finally derives from a pair of simultaneous equations with unknown $[p_2/p_1]^2$ and M_1. However, these equations cannot be solved explicitly in the form

given. Thus, a graphical method was used in which Eqs. (6) and (8) (mixing process case) or (10) and (14) (vortex sheet case) were each solved for $[R_2/R_1]^2$ with both results being plotted as a function of M_1, as shown in the sketch below. The intersection point is a solution with the corresponding M_1 and $[R_2/R_1]^2$ satisfying the simultaneous equations. A solution was thus determined for each assumed secondary flow rate.

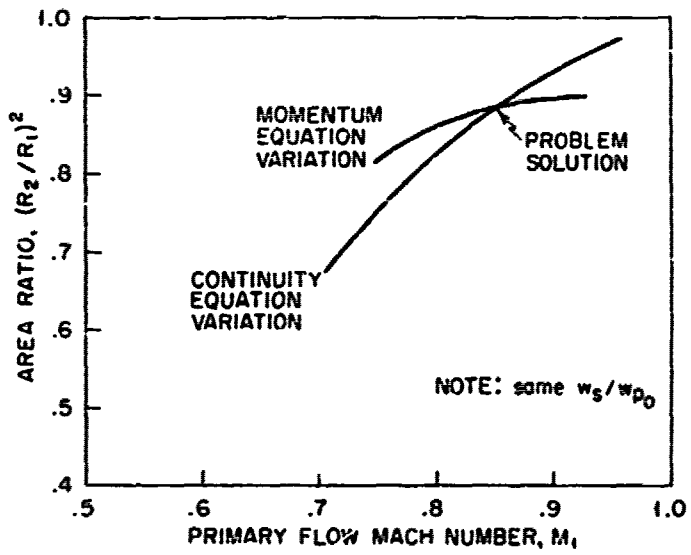

The most meaningful form of the results for both analytical models is one which directly indicates flow throttling performance. This is readily achieved when primary flow is given as a function of secondary flow. The area ratio $[R_2/R_1]^2$ found from the procedure above is a flow throttling parameter in both models. The continuity equation (Eq. 6) for the mixing process case shows that

$$\left[\frac{R_2}{R_1}\right]^2 = \frac{w_p + w_s}{w_{p_0}} \qquad (17)$$

Thus the primary flow throttling, a ratio of w_p/w_{p_0}, is determined by subtracting the associated value of w_s/w_{p_0} (assumed with M_{1_s}) from $[R_2/R_1]^2$. In the vortex sheet case, Eq. (10) shows that

$$\left[\frac{R_2}{R_1}\right]^2 = \frac{w_p}{w_{p_0}} \tag{18}$$

since the primary and secondary streams flow without mixing.

The results for the mixing process and the vortex sheet case are shown in Fig. 6 where primary flow ratio is plotted against secondary flow ratio. The corresponding data obtained by Martin is also shown. It is obvious from Fig. 6 that the data does not corroborate the theory. However, without closer inspection the data seems to have some similarity to the shape of the mixing process curve. This is contrary to the expectations of Martin who felt that, as the secondary flow increases, the flow configuration should depart from the mixing process form to become one of a vortex sheet character. The monotonically increasing difference in flow throttling between the mixing process and vortex sheet cases is due to the third term on the right hand side of Eq. (14). This term represents the secondary stream momentum at station 2 in the vortex sheet model and it increases continuously with increasing secondary flow rate.

A few criticisms of the Martin flow models may be made immediately as suggestions for sources of the disagreement shown in Fig. 6. The first and most obvious one is the absence of viscous effects. However, viscosity must be neglected with the hope of justification on the grounds that the resultant solvable problem will yield a useful solution. If such is not the case, then a more empirical method may be the only eventual practical approach. One assumption in both flow configurations which deserves comment is that the local injection conditions (pressure, density, temperature) are equal to the stagnation values in the primary stream. This implies that the primary stream is instantaneously at rest at the injection station. However, it is obvious that the primary stream velocity (at injection station) will be small only when the effective primary throat is reduced significantly by a good deal of throttling. In other words, the

assumption appears to be a poor one at low values of secondary flow rate. Furthermore, this assumption leads to somewhat unrealistic behavior of the secondary flow parameters. That is, by Eq. (16) (with fixed b_t/R_t and M_2) w_s/w_{p_0} is directly proportional to M_{1_S} which means that each secondary flow rate also has a different p_{0_S} and T_{0_S}. In addition, when M_{1_S} exceeds unity, each flow rate has a different size throat upstream of the entrance slot. This matter will be discussed further in the beginning of the section on NSL theory.

The data obtained by Martin is similar to some of the NACA data discussed earlier. A comparison is made in Fig. 7 where the appropriate flow throttling data is plotted. It should be pointed out that in addition to the differences noted in Fig. 7, the Martin data was obtained with a cylindrical channel while the NACA experiments were concerned with a convergent nozzle. Nevertheless, the curves in Fig. 7 show at least qualitative agreement between the experiments.

4. Summary

The work done by Martin must be recognized as an important contribution to the solution of the secondary injection problem. It was the first thorough attempt to generate a theoretical model of the flow throttling process. Although the analytical models devised by Martin were not well substantiated by experimental data, the methods involved were certainly worthy of study. In fact, that this was the case is demonstrated by the next section. It is shown therein that study of the Martin methods led to development of the NSL theoretical models which have been corroborated by experimental data.

B. NSL THEORY

The data from a series of NSL experiments (Phase I), like the Martin data, disagreed with the results of the Martin analytical models. This further evidence suggested that either the Martin hypotheses be improved or some others be developed. An effort was undertaken with these objectives and both have been achieved to an encouraging extent.

Two areas of effort were responsible for the analytical work accomplished. One is the water table study, which is described in the first portion of this section. The other is the further investigation of the Martin models, which is discussed in the second portion of this section.

The water table study and extended Martin work led to the final development of the NSL flow models. These are presented in the final portion of this section.

1. Water Table Study

In anticipation of further and more detailed research with air models (experimental), an experimental study was carried out to test the applicability of the hydraulic analogy (Ref. 5) to the flow throttling problem. It was felt that this technique might contribute some understanding at very little cost or experimental complexity.

A simple model was built based on the analogy. In a few words, the hydraulic analogue is the water flow through a horizontal channel which simulates the flow of a perfect gas with a γ of 2. The primary nozzle was a convergent-divergent one with an exit-to-throat area ratio corresponding to a Mach number of 3.0. In the flow through the nozzle, according to the analogy, the water height is proportional to the density and temperature in the gas while the gas pressure is proportional to the square of the water height. The secondary flow was injected (from a slot) at the throat of the primary nozzle, as it was in the previous series of experiments with air (Phase I).

The only measurements, aside from flow observations, obtained from this test were primary and secondary flow rate data. However, it was found that the water table data indicated essentially the same flow throttling variation as the one obtained with air. Thus, despite the comparison of two-dimensional data (water table) and three-dimensional data (Phase I, air) the analogy appeared to hold much better than had been anticipated.

In spite of a lack of understanding (which still exists) of the process which made the analogy hold so well, plans were formulated for

more refined and extensive tests. These studies were to be done on a larger water table at the MIT Hydrodynamics Laboratory. However, two-dimensional tests of the same kind, but using air, were found to look similarly attractive (due to existing NSL equipment) and offered the use of the NSL schlieren capability. In addition, it was felt that such data would be more directly applicable to an axisymmetric air nozzle. Thus, the water table method was abandoned in favor of two-dimensional air tests.

Nevertheless, the relatively crude experiments of the NSL water table did contribute to the effort. These tests were fruitful in that the flow observations helped to evolve the analytical models discussed in the remaining parts of this section. In particular, the water table flow showed that all of the throttling took place in a relatively short axial distance. This was regarded as support for the use of a constant-area channel flow analysis. In addition, the use of ink (as a visual aid) in the flow pointed the way toward the secondary flow behavior used in the NSL flow analyses.

2. Martin Models

The Martin analytical flow models, discussed in the preceding section, were studied beyond the work reported in Ref. 3. These studies had the objective of improving the analytical results and, in particular, correlating the NSL experimental data (Phase I) which is presented in a subsequent section.

The mixing process and vortex sheet cases were derived in the notation of the previous section, but according to some new assumptions. The assumption of local injection conditions (p, ρ, T) being equal to the primary stagnation values was modified. The implications of this assumption were mentioned on page 20. Although these implications might be considered acceptable for very small secondary flows (up to $w_s/w_{p_0} \sim 0.05$), they become unrealistic at higher (up to $w_s/w_{p_0} \sim 0.15$) but still reasonable levels. Nevertheless, to maintain the basic nature of the Martin approach, it was assumed that the local primary static pressure equals the local injection pressure

In addition, a new assumption was made regarding secondary injection. It was assumed that the secondary stream flows through a sonic orifice of fixed area from a reservoir at some stagnation pressure and stagnation temperature.* Furthermore, it was assumed that the injection station was at the sonic point of the unrestricted primary flow. The sonic orifice assumption simplifies the secondary mass flow equation but it means that the secondary-to-primary stagnation pressure ratio has a lower limit of one (for theoretical calculations). Since the secondary stagnation temperature is a constant (constant ratio to the primary value), the secondary flow rate varies in proportion to the stagnation pressure.

It was felt that these conditions were more realistic than those of Ref. 3.

a. Secondary Flow

The secondary flow rate, as in the previous section, is governed by the same equation in both the vortex sheet and mixing process cases. However, the exact form of the secondary flow ratio is now given as

$$\frac{w_s}{w_{p_0}} = \frac{\frac{A_{*s}}{\pi R_1^2}\left[\frac{\rho_{*s}}{\rho_{0_s}}\right]\left[\frac{\rho_{0_s}}{\rho_0}\right]\left[\frac{T_{*s}}{T_{0_s}}\right]^{\frac{1}{2}}\left[\frac{T_{0_s}}{T_0}\right]^{\frac{1}{2}}}{\left[\frac{\rho_2}{\rho_0}\right] M_2 \left[\frac{T_2}{T_0}\right]^{\frac{1}{2}}} \qquad (19)$$

which is based on the new assumptions relevant to the secondary flow. This equation also assumes, as before, that the primary and secondary fluids are the same gas.

*Thus, the sketches of the Martin flow configurations in the preceding section are still relevant with only slight modification. The flow now enters the channel through a sonic orifice of area A_{*_s} rather than an entrance of width b_1. Accordingly, the area of the secondary flow, in the vortex sheet case, is A_{2_s} at station 2.

b. Mixing Process Case

The important features of the mixing process case are shown in the sketch on page 13 except for the changes noted above. The continuity equation, analogous to Eq. (6), is

$$\left[\frac{p_2}{p_0}\right]\left[\frac{R_2}{R_1}\right]^2 M_2 \left[\frac{T_2}{T_0}\right]^{\frac{1}{2}} = \left[\frac{p_1}{p_0}\right] M_1 \left[\frac{T_1}{T_0}\right]^{\frac{1}{2}}$$

$$+ \frac{A_{*_s}}{\pi R_1^2}\left[\frac{p_{*_s}}{p_{0_s}}\right]\left[\frac{p_{0_s}}{p_0}\right]\left[\frac{T_{*_s}}{T_{0_s}}\right]^{\frac{1}{2}}\left[\frac{T_{0_s}}{T_0}\right]^{\frac{1}{2}} \qquad (20)$$

in which the secondary flow term is the same as that in Eq. (19). Furthermore, this term is, of course, the one which makes the equation different from Eq. (6).

The momentum equation is the same as Eq. (8) except for one term and is written as

$$\frac{p_1}{p_0}\left[1 + \gamma M_1^2\right] - \gamma M_{1_s}^2 \left[\frac{A_{1_s}}{A_{*_s}}\right]\left[\frac{A_{*_s}}{\pi R_1^2}\right]\left[\frac{p_{1_s}}{p_{0_s}}\right]\left[\frac{p_{0_s}}{p_0}\right] \cos\phi$$

$$= \frac{p_2}{p_0}\left[1 + \gamma M_2^2 \left(\frac{R_2}{R_1}\right)^2\right] \qquad (21)$$

where A_{1_s}/A_{*_s} is the isentropic area ratio which corresponds to M_{1_s}.* Hereafter, M_{1_s} denotes the Mach number to which the secondary flow is

*The isentropic flow area ratio is a form of the continuity equation for a perfect gas and is given by

$$\frac{A}{A_*} = \frac{1}{M}\left[\frac{2}{\gamma+1}\left(1 + \frac{\gamma-1}{2} M^2\right)\right]^{\frac{\gamma+1}{2(\gamma-1)}}$$

in which M is the Mach number at the station where A is the area, in a streamtube flow.

assumed to accelerate as it enters the primary nozzle. The injection Mach number is unity since, by definition, the secondary flow is exhausted from a sonic orifice. As before, it is assumed that the average stagnation density of the combined stream is equal to the initial primary stagnation density.

c. Vortex Sheet Case

The vortex sheet flow configuration is shown by the sketch on page 15 except for the changes noted on page 24. The continuity equation is the same as Eq. (10). The continuity equation for the secondary flow is treated below.

The momentum equation, analogous to Eq. (14), is

$$\frac{p_1}{p_0}\left[1+\gamma M_1^2\right]-\gamma M_{1_s}^2\left[\frac{A_{1_s}}{A_{*_s}}\right]\left[\frac{A_{*_t}}{\pi R_1^2}\right]\left[\frac{p_{1_s}}{p_{0_s}}\right]\left[\frac{p_{0_s}}{p_0}\right]\cos\phi$$

$$=\frac{p_2}{p_0}\left[1+\gamma M_2^2\left(\frac{R_2}{R_1}\right)^2\right]+\gamma M_{2_s}^2\left[\frac{A_{2_s}}{A_{*_s}}\right]\left[\frac{A_{*_s}}{\pi R_1^2}\right]\left[\frac{p_{2_s}}{p_{0_s}}\right]\left[\frac{p_{0_s}}{p_0}\right] \quad (22)$$

where A_{2_s}/A_{*_s} is the isentropic area ratio* which corresponds to M_{2_s} from secondary flow continuity considerations. The secondary Mach number M_{2_s} is determined, as before, by p_{2_s}/p_{0_s} according to the procedure on page 17.

d. Flow Throttling Results

The flow models developed above are analogous to those of the preceding section and essentially the same final assumptions are required for a problem solution. It is also obvious that these assumptions result in a similar final set of simultaneous equations.

It was assumed, as in the previous instance, that the overall primary pressure ratio ($p_2/p_0 = 0.5283$) was such that $M_2 = 1$. Also,

*See footnote on page 25.

air was again the working fluid in both the primary and secondary streams. The secondary-to-primary stagnation temperature ratio was assumed to be unity, which reduces Eq. (19) to

$$\frac{w_s}{w_{p_0}} = \frac{p_{0_s}}{p_0} \times \frac{A_{*_s}}{\pi R_1^2} \qquad (23)$$

The value of $A_{*_s}/\pi R_1^2$, analogous to $2b_1/R_1$, was chosen somewhat arbitrarily as 0.05. The injection angle ϕ was taken as 60° since this was the angle peculiar to the NSL Phase I tests. The resultant sets of simultaneous equations for the two flow models were again solved by the graphical technique presented on page 19.

The results for the mixing process and vortex sheet cases are shown in Fig. 8 where primary flow ratio is plotted against secondary flow ratio. It is not possible, as mentioned previously, to generate meaningful results at a p_{0_s}/p_0 of less than one, which by Eq. (23) corresponds to a w_s/w_{p_0} of less than 0.05. Thus, the solid curves begin at this value of secondary flow ratio. Over the comparable range of secondary flow rates, the previous corresponding results of Fig. 6 show reasonable similarity considering the parametric (injection area, ϕ) differences. However, at higher flow rates the method of Ref. 3 (corresponding to results in Fig. 6) yields significantly more flow throttling than that shown in Fig. 8. This difference in performance can be traced to the assumption which concerns local injection conditions. The NSL (Phase I) data corresponds to significantly less flow throttling than the prediction of the method of Ref. 3. Thus, the modifications which correspond to the decreased flow throttling results of Fig. 8 may be regarded as improvements in the Martin models.

3. NSL Flow Models

Further study led to modifications of the Martin flow models which then yielded results that proved to correlate the NSL data. In addition to the improvement in the Martin models, a new one was developed which is also supported by the experimental results.

The major modification of the Martin models is a difference

in the treatment of the stagnant air zone (see sketches on pages 13 and 15). It was felt that this separated flow zone might exist at some very low pressure. That is, the centrifugal force on the secondary flow as it changes direction (by $\pi - \phi$) might leave little flow near the wall just downstream of the injection point. Therefore, for the purposes of analysis, it was assumed that the separated flow zone pressure is negligible (mathematically, zero) compared to that in the primary and secondary streams. The resultant flow models are called the "secondary mixing" case (modified mixing process case) and the "sheet flow" case (modified vortex sheet case).

The detailed development of the secondary mixing and sheet flow cases is given below. Also presented is the development of the third model which is called the secondary expansion case.

a. Secondary Flow

The secondary flow ratio is given by Eq. (19) for the secondary mixing, sheet flow, and secondary expansion flow models. In all three cases, the assumption is again made that the primary and secondary fluids are the same gas.

b. Secondary Mixing Case

The secondary mixing flow configuration is shown by the sketch on page 13 as modified by the remarks on page 24. The appropriate form of the continuity equation is given by Eq. (20).

The momentum equation, similar in form to Eq. (21), is written in the present case as

$$\frac{p_1}{p_0}\left[1 + \gamma M_1^2\right] - \gamma \left[\frac{A_{*s}}{\pi R_1^2}\right]\left[\frac{p_{*s}}{p_{0_s}}\right]\left[\frac{p_{0_s}}{p_0}\right]\cos\phi$$

$$= \frac{p_2}{p_0}\left(\frac{R_2}{R_1}\right)^2\left[1 + \gamma M_2^2\right] \qquad (24)$$

This equation has the additional assumption that the entering secondary flow does not expand to supersonic speed. That is, it does not accelerate along the original entrance direction. This is believed to be a more realistic assumption and it is supported by observations of the water table flow. The pressure ratio p_{*_s}/p_{0_s} is thus a constant (sonic value of 0.5283) with M_{1_s} being equal to unity. Finally, it is again assumed that the average stagnation density of the combined stream is the same as the initial primary stagnation density.

c. Sheet Flow Case

The flow configuration for the sheet flow case is shown in the sketch on page 15 as modified by the remarks on page 24. The sheet flow case continuity equation for the primary flow is the same as Eq. (10).

The momentum equation for the sheet flow case is given by

$$\frac{p_1}{p_0}\left[1+\gamma M_1^2\right]-\gamma\left[\frac{A_{*_s}}{\pi R_1^2}\right]\left[\frac{p_{*_s}}{p_{0_s}}\right]\left[\frac{p_{0_s}}{p_0}\right]\cos\phi$$

$$=\frac{p_2}{p_0}\left(\frac{R_2}{R_1}\right)^2\left[1+\gamma M_2^2\right]+\frac{p_2}{p_0}\left[\frac{A_{2_s}}{A_{*_s}}\right]\left[\frac{A_{*_s}}{\pi R_1^2}\right]$$

$$+\gamma M_{2_s}^2\left[\frac{A_{2_s}}{A_{*_s}}\right]\left[\frac{A_{*_s}}{\pi R_1^2}\right]\left[\frac{p_{2_s}}{p_{0_s}}\right]\left[\frac{p_{0_s}}{p_0}\right] \qquad (25)$$

where, as in the secondary mixing case, it is assumed that the entering secondary flow does not expand to supersonic speed. Also, A_{2_s}/A_{*_s} is the isentropic area ratio* which corresponds to M_{2_s} from secondary flow continuity considerations. The secondary Mach number M_{2_s} is again determined by p_{2_s}/p_{0_s} as shown on page 17.

*See footnote on page 25.

d. Secondary Expansion Case

In the secondary expansion model the flow behavior is somewhat different from either of the preceding cases. The secondary flow enters the nozzle, as in the preceding models, through a sonic orifice and is directed similarly, at an angle of injection ϕ. In addition, the primary and secondary streams, as in the sheet flow case, do not mix as they flow downstream. However, in the present model the secondary stream expands as it flows to station 2 (see sketch on page 15), filling the region between the wall and the primary stream. Furthermore, the secondary flow expansion is isentropic and the Mach number M_{2_s} is given by the isentropic area ratio A_{2_s}/A_{*_s}. Thus the secondary expansion model assumes that the secondary stream does not separate from the wall.

The continuity equation for the present case is the same as that of the sheet flow one, namely, Eq. (10). The momentum equation is

$$\frac{p_1}{p_0}\left[1+\gamma M_1^2\right]-\gamma\left[\frac{A_{*_s}}{\pi R_1^2}\right]\left[\frac{p_{*_s}}{p_{0_s}}\right]\left[\frac{p_{0_s}}{p_0}\right]\cos\phi$$

$$=\frac{p_2}{p_0}\left(\frac{R_2}{R_1}\right)^2\left[1+\gamma M_2^2\right]+\left[\frac{p_{2_s}}{p_{0_s}}\right]\left[\frac{p_{0_s}}{p_0}\right]\left[1+\gamma M_{2_s}^2\right]\left[1-\left(\frac{R_2}{R_1}\right)^2\right] \quad (26)$$

where the area ratio A_{2_s}/A_{*_s}, which determines M_{2_s}, is obtained from

$$\frac{A_{2_s}}{A_{*_s}}=\frac{\pi\left(R_1^2-R_2^2\right)}{A_{*_s}}=\frac{\left[1-\left(\frac{R_2}{R_1}\right)^2\right]}{\frac{A_{*_s}}{\pi R_1^2}} \quad (27)$$

Since A_{2_s}/A_{*_s}, and thus M_{2_s}, depends on $(R_2/R_1)^2$, a trial value is needed for the $(R_2/R_1)^2$ in Eq. (27) in order to solve Eq. (26) for the same parameter. However, as mentioned on page 18, the area ratio $(R_2/R_1)^2$ found

from the continuity and momentum equations (Eqs. 10 and 26, respectively) is determined for various assumed values of M_1. Thus, in the present case the assumed M_1 yields an $(R_2/R_1)^2$ from Eq. 10 (continuity) which is then used as a trial value in Eq. (27) so that Eq. (26) (momentum) may also be solved for $(R_2/R_1)^2$. The M_{2_s} corresponding to the A_{2_s}/A_{*_s} in Eq. (27) is used to obtain the pressure ratio p_{2_s}/p_{0_s}.

e. Flow Throttling

The three flow models developed above yield problem solutions in the manner described previously on page 18. The solutions depend on certain final assumptions and these were the same as those of section 2d. In particular, the overall primary pressure ratio p_2/p_0 was assumed to be 0.5283 ($M_2 = 1$) and air was the fluid in the primary and secondary streams. In addition, the secondary-to-primary stagnation temperature ratio was assumed to be unity which means Eq. (23) determines the secondary flow ratio. Firally, the injection angle ϕ was taken as 60° while the area ratio $A_{*_S}/\pi R_1^2$ was assumed to be 0.05.

The results for the secondary mixing, sheet flow, and secondary expansion models are shown in Fig. 9. Also shown, for purposes of comparison, are the curves of Fig. 8. It is apparent that the comparable flow models (secondary mixing versus mixing process and sheet flow versus vortex sheet) yield very different flow throttling performance. The difference between them results from the new treatment of the separated flow region as well as the assumption that there is no acceleration of the entering secondary flow. The major portion of this difference, however, is due to the assumption of a negligible pressure in the separated flow zone.

The difference between the mixing process and secondary mixing cases is seen to be smaller than the difference between the vortex sheet and sheet flow cases. Although this effect is a direct result of the consideration of the separated flow region, it may be traced to a more basic reason. This reason is a two-sided one which involves an assumption in the mixing process and secondary mixing models as well as an inherent feature of the vortex sheet and sheet flow models. The effect in question

is a result of the assumption that the average stagnation conditions, in the mixing process and secondary mixing cases, are the same as the initial values in the primary stream. On the other hand, the vortex sheet and sheet flow models cannot require an analogous assumption since the primary and secondary flows are considered separately. Furthermore, the assumption in the mixing models means that the results must become somewhat unrealistic at high secondary flow rates.

Although specific comparisons to experimental data follow in another section, it was found that the sheet flow and secondary expansion cases encompassed almost all of the data. This seems very reasonable since these flow models are, in a sense, two extremes, of a type of flow behavior. In the sheet flow case the secondary stream flows in a sheet circumjacent to the primary stream. Thus, the secondary pressure (at station 2 in the analysis) is determined by the primary stream and, since the change in flow direction (120°) is large, the secondary stream is separated from the nozzle wall. In the secondary expansion case, however, the secondary stream expands to fill the area between the primary stream and the wall. In this case the secondary pressure is independent of the adjacent primary value and there is no separated flow region. The water table observations indicated that both flow configurations exist simultaneously (separation upstream of secondary expansion zone) and, if the air data may be taken as proof, this may actually be the case.

Finally, it should be pointed out that the sheet flow and secondary expansion models seem to be capable of taking account of temperature effects. As shown on page 4, hot and cold gas data were found to vary in the same direct proportion to secondary flow ratio times $\left[T_{0_s}/T_0\right]^{\frac{1}{2}}$. The throttling performance of the sheet flow and secondary expansion flow configurations is similarly related to secondary flow. The secondary-to-primary stagnation temperature ratio does not appear in the continuity equation (Eq. 10) or in the momentum equations (Eqs. 25 and 26) of either model. Thus, for a given secondary-to-primary stagnation pressure ratio, throttling performance is specified. However, according to Eq. (19)

the secondary flow ratio becomes

$$\frac{w_s}{w_{p_0}} = \left[\frac{A_{*s}}{\pi R_1^2}\right]\left[\frac{p_{0_s}}{p_0}\right]\left[\frac{T_0}{T_{0_s}}\right]^{\frac{1}{2}}$$

which means that the secondary flow for a given throttling level is proportional to the stagnation temperature ratio. Furthermore, it is obvious that if the secondary flow ratio is multiplied by $[T_{0_s}/T_0]^{\frac{1}{2}}$ then throttling performance is independent of temperature ratio and related to the parameter

$$\frac{w_s}{w_{p_0}}\left[\frac{T_{0_s}}{T_0}\right]^{\frac{1}{2}}$$

by a constant.

SECTION IV

EXPERIMENTAL RESULTS

The initial phase of the NSL effort took the form of a series of experiments in which secondary injection was used in an axially symmetric nozzle. A variety of injection configurations were tested with air as the working fluid in both the primary and secondary streams. The objective of the program was to determine some of the flow throttling and thrust control characteristics peculiar to the injection method. These tests are the primary concern of this section of the report. The first portion of this section is devoted to a descriptive discussion of the model and test conditions. The remainder of this section is a presentation of the test results.

A. MODEL DETAILS AND TEST CONDITIONS

1. Air Supply System

The supply systems for both primary and secondary air are shown in the schematic diagram of Fig. 10. Air for the primary flow was pumped by Chicago Pneumatic Compressors through a drier into three storage tanks denoted as receivers. As it flowed from the receivers, the air was throttled by the main control valve before flowing through a surge tank to the primary flowmeters. The flowmeters were used to measure the mass flow of primary air flowing through the model. After passing through the flowmeters, the air passed through a bellows system and into the model settling chamber. A thermocouple located just upstream of the flowmeters was used to obtain the stagnation temperature of the primary air. A 150 psia Heise gage was used to measure the primary stagnation pressure. This stagnation pressure was maintained at a constant level regardless of the amount of primary flow throttling. The primary stagnation pressure (p_0) was 100 psia in nearly all of the runs in the test program (exceptions: 75 psia and 50 psia).

The secondary air, during most of the tests, was obtained from banks of standard air bottles having an initial pressure of 2500 psi. For the last group of runs, however, a storage tank and compressor (1500 psi outlet pressure) replaced the bottled air supply. Both sources delivered air to the same pressure regulating system. Two manually operated secondary flow control valves, downstream of the flowmeter, were used to obtain the desired secondary stagnation pressure which was measured with a 3000 psia Heise pressure gage. As in the primary flow, a Rubicon potentiometer was used to measure the output of a stagnation temperature thermocouple located upstream of the flowmeter The secondary air flowed through a pair of flexible hoses before entering the model secondary settling chamber.

2. Model Arrangement

The model arrangement is shown in some detail in Fig. 11a. Strain gage techniques were employed to measure directly the forces of interest on the model. Nozzle thrust was measured with the NSL wall balance, and a pair of balances mounted on either side of the model determined side force magnitude and position.

The primary air flowed through four bellows in a system designed to transmit a minimum of interference forces to the model. As shown in Fig. 11b, each bellows had a pair of thin axial restraints mounted on either side. These restraints restricted bellows distortion while allowing model displacement (due to thrust) to occur without opposition. After passing through the bellows, the primary air flowed into the model through a tee designed to give a minimum resultant net force on the model.

The weight of the model system shown in Fig. 11a was supported by a counterweight so that only small tare forces acted on the moment balances with no flow through the model. A long cable and pulley were used in the counterweight system so that the only resistance to thrust took the form of a small friction force in the pulley.

The strain gage balance calibrations were performed with the secondary air system pressurized and primary air flow ranging from

zero to the maximum design value of one pound per second. During calibration runs a specially designed pipe tee replaced the nozzle in the model. This tee exhausted the primary air in directions normal to the model axis in an effort to minimize interference forces which would affect the thrust calibration. Similarly, a negligible effect on the side force calibration was obtained by the exhaust of equal flows in opposition to one another (a drawing of the nozzle details showing the tee location is shown in Fig. 12).

The results of the thrust calibration indicated that the primary flow had essentially no effect on the measurements. This is attributed to the flexibility of the bellows system. Thrust effect on side force was appreciable but this was unavoidable due to the thrust force being transmitted to the wall balance by the side force balances.

A photograph of the model installation is shown in Fig. 13.

3. Nozzle Design

The details of the nozzle portion of the model are shown in Fig. 12. The primary nozzle was conical and designed to expand the flow to atmospheric pressure. The design flow rate was one pound per second with a stagnation pressure of 100 psia and a stagnation temperature of 530°R. The exit Mach number of the nozzle, according to the exit-to-throat area ratio, was 2.1.

The complete nozzle was assembled from three separate pieces with the bolted back plate holding the assembly in its proper orientation. The central portion of the nozzle was changed for each new injection configuration. Two static pressure taps were located near the nozzle exit.

A pressure tap in the wall of the primary settling chamber measured the primary flow stagnation pressure while a pressure tap in the outside wall of the secondary settling chamber was used to measure the secondary flow stagnation pressure. This secondary stagnation pressure was varied between 70 and 300 psia. The injection area was such that a pressure of 300 psia produced a secondary flow of about 0.15 lb per second. The primary stagnation pressure (100 psia) and

nozzle throat area (0.430 in.^{2}) resulted in an unrestricted (no flow throttling) primary flow of approximately 1 lb per second.

4. Injection Configurations

The significant configurations that were tested are described below by the pertinent information concerning orifice geometry, etc.

Configuration*	No. Holes	Hole Dia. (in.)	ϕ (deg.)	Slot Width (in.)
C	16	0.032	90	———
D	16	0.032	60	———
E	8	0.032	60	———
F	32	0.032	60	———
G	16	0.0465	60	———
H	32	0.032	60	———
	Same as F except that injection holes are slightly upstream of nozzle throat			
J	—	———	60	0.020
J_r	Same as J except that injection is from two diametrically opposite quadrants			
K	52	0.0292	60	———
L	16	0.0465	60	———
	Diameter given corresponds to throat of nozzle shaped holes with a design injection (exit) Mach number of 1.8. These holes exhausted air at a station slightly upstream of the throat.			

*Unless otherwise specified all orifices are at the nozzle throat and equally spaced around the circumference. The injection angle, as defined previously, is the angle included between the primary nozzle axis and the axis of injection. Unless otherwise specified p_0 = 100 psia.

Configuration	No. Holes	Hole Dia. (in.)	δ (deg.)	Slot Width (in.)
L_r	8	0.0465	60	———
M	32	0.032	60	———
	The primary nozzle shape was modified to produce a slightly smaller pressure gradient in the throat region. In addition, the injection holes were located slightly upstream of the throat.			
M_{r_1}	16	0.032	60	———
M_{r_2}	16	0.032	60	———
	Primary stagnation pressure (p_0) = 75 psia.			
M_{r_3}	16	0.032	60	———
	Primary stagnation pressure (p_0) = 50 psia.			

There were a few additional configurations tested which are not listed above. In these configurations secondary air was injected at a station about two thirds of the throat radius upstream of the throat. Since the results obtained were not significant, no further mention of these configurations will be made.

The asymmetric injection configurations tested were merely modifications of the ones that appear in the above table. As shown in Fig. 12, the secondary air flowed through threaded holes before being exhausted from the various types of injection orifices. Therefore, to produce asymmetric injection, screws and sealing gaskets were used which blocked the passage of flow to various holes. Configurations C, D, F, G, L, and J were so modified to obtain asymmetric injection data.*

*The subscript s is used to denote an asymmetric injection configuration (for example, F_s).

B. TEST RESULTS

1. Flow Throttling

The experimental flow throttling performance of the various configurations in the Phase I program is presented in the following paragraphs. The data is compared to the corresponding theoretical results for the sheet flow and secondary expansion configurations.

A few words of explanation are in order concerning the analytical model flow calculations. The basis of the theoretical calculations was the same for every injection configuration. It was assumed, for instance, that the flow throttling which occurred in the nozzle (shown in Fig. 12) took place in a relatively short axial distance. Thus, the primary pressure ratio was taken as $p_2/p_t = 0.5283$ ($M_2 = 1$) and the throat area (0.430 in.^{2}) was assumed to be πR_1^2. In all cases, of course, air was the working fluid in the primary and secondary streams. The measurements of primary and secondary stagnation temperatures (about 530°R) indicated that, for analytical calculation purposes, a value of unity was a good approximation for the secondary-to-primary stagnation temperature ratio. Since the analytical methods do not contain an orifice coefficient (C) in the secondary mass flow equation, the area ratio $A_{s_s}/\pi R_1^2$ was replaced, in the analytical calculations,* by $C\,A_{s_s}/\pi R_1^2$. This procedure was adopted, somewhat arbitrarily, so that the theoretical and experimental stagnation pressure ratios p_{0_s}/p_0 would be about the same for a given w_s/w_{p_0}. The value of δ was 60° in every configuration except one (see configuration list on page 38).

The flow throttling results obtained with configurations C, D, E, and F are shown in Fig. 14.** Primary flow ratio is plotted against secondary flow ratio with the data normalized by the w_{p_0} value appropriate to the particular configuration. This plot shows configurations in

---

* An approximation to the average value of C was used for each configuration.

** The experimental uncertainties (for all of the Phase I data) in the flow measurements are ±0.01 in w_p/w_{p_0} and ±0.003 in w_s/w_{p_0}.

all of which the injection orifices are holes 0.032 inches in diameter. It is apparent that the agreement between theory and experiment is not very good at $\phi = 90°$ However, at $\phi = 60°$ the data appears to corroborate the theoretical models. This difference in performance might be the result of a shorter axial distance in which throttling takes place, produced by a ϕ of 60° wherein the secondary flow is directed upstream. The number of injection holes evidently does not affect experimental agreement with the theoretical models.

In Fig. 15 the primary flow ratio of configurations F and H is plotted against secondary flow ratio. Configuration H is the same as F except for its injection orifices being effectively (nozzle contour slightly modified) moved to a position slightly upstream of the nozzle throat. There is essentially no difference in performance between these two configurations.

Primary flow ratio is plotted against secondary flow ratio for configurations G, L, and L_r in Fig. 16. Although the L configurations had injection orifices designed for supersonic flow, it is believed that such flow was never achieved. The p_{t_s}/p_0 pressure ratios actually run were too low to fill the orifice nozzle with supersonic flow.* Furthermore, the flow throttling of the L configurations is essentially the same as that of the G one which has sonic injection orifices. In spite of the different (from that in Figs. 14 and 15) orifice diameter of 0.0465 inches, the data agrees with the corresponding results of the analytical models. In addition, the number of such holes (L with 16, L_r with 8) also does not affect agreement between theory and experiment.

Figure 17 shows the throttling performance of configurations K, J, and J_r. The primary flow variation with secondary flow is seen to be essentially the same for configurations K and J. This agreement indicates that there is no important difference between slot and orifice injection. Configuration J_r, in which flow was injected from opposite

*The analytical results therefore assumed that the entering secondary flow did not expand to supersonic speed.

quadrants of the slot, yields the same throttling variation as that of J. This result shows a rather surprising independence of performance from the injection arrangement. All of the data in Fig. 17 shows good agreement with the analytical results.

The flow throttling performance of configurations F, M, and M_{r_1} are compared to the corresponding analytical results in Fig. 18. The theoretical models are apparently substantiated by the experimental data. In these configurations the injection orifices are 0.032 inch diameter holes but the nozzle contour in the M case is modified as shown in the sketch below.

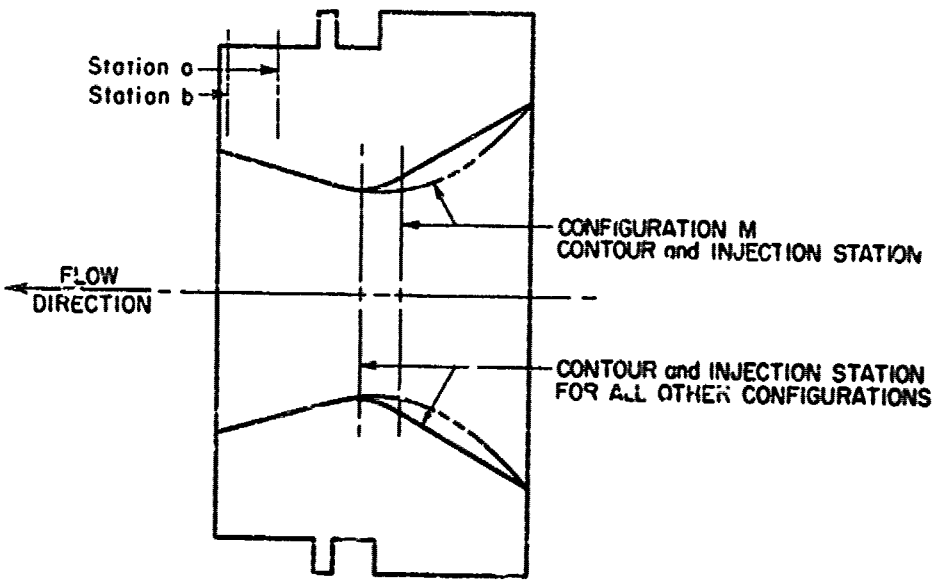

This M contour produces a slightly smaller pressure gradient in the throat region. Nevertheless, the throttling performance achieved by the M configuration is not significantly different from that of F, or, for that matter, M_{r_1}. Although the difference in throttling between M and F is negligible, it should be noted that the change in contour produces only a small decrease in the throat-region pressure gradient.

The lack of an effect of the number of orifices (as between M and M_{r_4}) agrees with the results above (in Figs. 14 and 16).

Configurations M_{r_1}, M_{r_2}, and M_{r_3} are compared to the appropriate analytical results in Fig. 19.* In all three cases the primary pressure ratio was assumed to be such that $M_2 = 1$, for the purposes of the theoretical calculations. The agreement of the data with the analytical results, in spite of the various primary stagnation pressures, seems to support the hypothesis that the throttling process takes place in a relatively short axial distance where the nozzle area can be considered approximately constant.

The flow throttling results for configurations F and J are shown in Fig. 20 where asymmetric injection is compared to symmetric injection. Although only configurations F and J are shown, results are similar with all of the others. It is obvious that asymmetric throttling is essentially the same as symmetric, on the basis of a given secondary flow rate. This result agrees with the one obtained with configuration J_r, and adds further evidence to the supposition that flow throttling is independent of the circumferential injection arrangement (β).

The data obtained with configuration J is compared to some NACA data in Fig. 21. All of the configurations are of the slot type with comparable injection areas. It is apparent that the NSL and NACA data are not considerably different. The smaller injection angle of the NSL data increases flow throttling while the higher pressure ratio (p_0/p_{atm}) has the opposite effect. However, as evidenced by the results cited above for configuration M_r, beyond a pressure ratio of about 3.4 this parameter does not seem to influence flow throttling. It is thus believed that in the present instance the difference in primary nozzles is of more importance than the primary pressure ratio. The NSL and NACA data are therefore reasonably similar with the difference attributable to the differences in injection angle and primary nozzle geometry.

---

*The primary stagnation pressures were 100, 75, and 50 psia for M_{r_1}, M_{r_2}, and M_{r_3}, respectively.

The results shown in Figs. 14 through 21 indicate that all of the configurations tested have approximately the same flow throttling characteristics. In addition, this flow throttling is significant compared to the variation which implies constant total nozzle flow. Theory agrees with experiment over a range of injection variables.

2. Thrust Control

The thrust of a conventional nozzle is directly proportional to the product of its mass flow and exit velocity. However, it was not known, a priori, to what extent secondary injection might affect this relationship. Furthermore, if the NSL theoretical work had been available prior to the tests, it might have been of little use for information about thrust variation.

The thrust measurements obtained in the Phase I test program are similar to those reported (and discussed in Section IIB) by the NACA in Ref. 1. That is, it was found that the thrust is proportional to the total (primary plus secondary) nozzle flow. The value of a thrust parameter defined as

$$\frac{\Gamma' T_0}{\frac{w_p + w_s}{w_{p_0}}}$$

was calculated for all of the significant test data. T_0 and T are the measured thrusts which correspond to the measured flow rates w_{p_0} and $w_p + w_s$, respectively. This thrust parameter was found to be between 0.96 and 1.04 in over 97 percent of the test runs (includes symmetric and asymmetric injection data). This range is somewhat higher than the thrust ratio (0.94 – 0.98) of the NACA data but the corresponding parameter (see page 7) is not the same as the one above. In fact, the difference in numerical results is believed to be due to the difference in definitions. The NACA thrust ratio would tend to be slightly smaller since the V_s involved increases with w_s.

Thus, it may be said that the NSL and NACA data are in close agreement on the proportionality of thrust to total nozzle flow. Furthermore, the proportion makes it appear that the exhaust velocity of the

nozzle remains essentially constant. Examination of particular data, however, shows a significant trend in the variation of thrust with total nozzle flow.

The thrust ratio T/T_0 and total flow ratio $(w_p + w_s)/w_{p_0}$ of configurations F, J, and K are shown as a function of secondary flow in Fig. 22.* The results shown are typical of asymmetric as well as symmetric injection configurations. Although it is not apparent in the case of configuration F, the others show an obvious difference between T/T_0 and $(w_p + w_s)/w_{p_0}$ which is an increasing function of secondary flow rate. Thus, it appears probable, and reasonably so, that there is a loss in exhaust velocity which increases with secondary flow. This might be considered as a loss in throttling efficiency from the viewpoint which seeks a maximum from the propulsive potential of the total nozzle flow.

In spite of the efforts (mentioned earlier) to make it otherwise, nozzle thrust and primary flow had a pronounced effect on the calibration of the side force balances. In fact, this effect was large enough so that a severe limit was imposed on the accuracy of the side force measurements. Nevertheless, asymmetric configurations were tested and a few qualitative remarks may be made about the corresponding results.

Configurations C, D, F, G, L, and J were modified, as mentioned previously, to permit side force evaluations. In these configurations injection took place over an arc of about one quarter or one half of the circumference. In all cases, the side force, as expected, was toward the side of the nozzle from which the secondary flow was injected.

The side force was found, as in the UAC and NACA tests, to be proportional to the secondary flow rate. However, the magnitude of the side force was discernible only to the extent that it was of the order of the secondary flow reaction force. The effect of the circumferential injection angle (β) was not ascertainable from the data.

3. Nozzle Pressures

The primary nozzle was instrumented with two pressure taps which were used to measure the static pressure near the nozzle exit.

*The experimental uncertainty in T/T_0 is approximately ± 1 percent.

The data obtained from configurations F and J, for symmetric and asymmetric injection, is plotted in Fig. 23 as a function of secondary flow ratio.* The data is connected by straight lines merely for the purpose of clarity. The data shown for these configurations is typical of the measurements corresponding to the other configurations. Station a is upstream of station b, and the pressure taps are axially in line with one another (see sketch on page 42). It is apparent that in the case of symmetric injection p_b increases or decreases only slightly with increasing secondary flow rate. In some cases it remains essentially constant. At station a, however, the static pressure tends to decrease with increases in secondary flow.

In sharp contrast to these effects are those of the data for asymmetric injection. It should be pointed out, however, that the pressure taps are located on the injection side of the nozzle at about the middle of the circumferential angle of injection (β). The asymmetric injection data shows a pronounced decrease in static pressure with increasing secondary flow rate. In spite of the apparent difference in the shape of the data between configurations F_s and J_s, the flow behavior in both is believed to be basically the same. In both configurations, asymmetric injection decreases the pressure downstream of the injection zone. Furthermore, this decrease evidently extends to the end of the nozzle since the downstream pressure tap is also affected. However, the J_s configuration, probably due to the difference in β, shows a significantly greater rate of pressure decrease than the F_s configuration. Thus, the subsequent rise in pressure, first at station b and then at station a, indicates that the flow separated (at least locally) from the nozzle wall. After separation, the pressures naturally approach the ambient atmospheric level ($p/p_0 \equiv 0.147$). The F_s configuration, in contrast, shows that separation did not take place since both pressures decreased in a monotonic fashion.

Also shown in Fig. 23, for purposes of comparison, are the pressure levels, at stations a and b, which correspond to isentropic,

*The experimental uncertainty in the nozzle pressure measurements is negligible on the scale shown in Fig. 23.

one-dimensional flow in the basic nozzle. The data shown is typical in that the measured pressures were equal to or lower than the ideal value at station a while the data at station b was always higher than the ideal value. The presence of the nozzle boundary layer tends to reduce the flow area and thus the Mach number. A lower Mach number corresponds to a higher pressure such as that shown at station b. However, the same effect is not evident at station a since the local acceleration of the flow at the wall in the throat region (where the nozzle shape makes the flow two-dimensional) extends some distance downstream.

The decreases in static pressure shown in Fig. 23 suggest certain possibilities with regard to flow behavior. Such a decrease in static pressure seems to indicate a local acceleration of the flow at least near the wall. However, the opposing effects of viscous losses and increasing secondary stagnation pressures may change p_0 from the constant value of 100 psia assumed in Fig. 23. Furthermore, the flow at the wall may be mostly secondary flow as part of a large injection zone which extends downstream from the nozzle throat. Nevertheless, it appears that the flow at the wall may be accelerated downstream of the injection station. In the case of symmetric injection the flow acceleration (compared to $w_s = 0$) might be followed by a weak shock wave between stations a and b (area ratios A/A_* of approximately 1.47 and 1.81, respectively). This would explain the decrease of static pressure at station a being greater than that at station b. In the case of asymmetric injection the process might be similar but amplified in the region local to injection, i.e., directly downstream of the injection zone. That is, the decrease in β for a given secondary flow rate might produce a greater region of disturbed flow. The corresponding increase in local acceleration would then explain the greater (compared to symmetric injection) decrease in static pressure. Furthermore, the increased region of disturbed flow might also move the shock wave downstream. This would then explain the behavior of the asymmetric injection pressure measurements.

SECTION V

CONCLUSIONS AND FUTURE WORK

The theoretical and experimental results presented herein lead to certain conclusions regarding thrust control with secondary injection.

1. A relatively simple analytical flow model was devised which assumes isentropic, one-dimensional flow in a constant area channel. This model yields flow throttling results which correlate the experimental data.

2. The flow throttling achieved with secondary injection is significant and roughly the same for all of the configurations tested. The reduction in primary flow is about $2\frac{1}{2}$ times the injected secondary flow.

3. Flow throttling is insensitive to the orifice arrangement (slot versus holes, etc.) in symmetric and asymmetric injection.

4. Flow throttling is not changed by variations in the overall primary pressure ratio when the level is in the supersonic range.

5. Overall primary pressure ratios in the transonic range increase the sensitivity of flow throttling to injection area.

6. Flow throttling varies significantly with injection angle (ϕ).

7. The circumferential angle of injection (β) has no effect on flow throttling (based on a given secondary flow rate).

8. Primary nozzle geometry is important but its importance is affected by the overall primary pressure ratio. The effect of geometry is attenuated by increasing primary pressure ratio.

9. Thrust is directly proportional to total nozzle flow. The proportionality constant, however, decreases slowly from a value of one with increasing secondary flow (for both symmetric and asymmetric injection).

The second major phase of NSL work began with an experimental study designed to investigate the basic nature of the injection process. According to original plans, the water table technique was to have been used for this experimentation. However, as mentioned in Section IIIB, this method was abandoned in favor of a two-dimensional gas model. Some tests have been performed with this type of model and the technique worked so well that it was decided to pursue the remainder of the investigation with this apparatus.

The remainder of work being planned is designed to study further the feasibility of thrust control with gas injection. The experimental portion will investigate the effects of injection angle (ϕ), throat region geometry and injection location. The analytical work presented herein will be modified, where necessary, to correlate additional data. In addition, the NSL analytical method will be used to predict results for real engine conditions (as the method permits) as well as others of interest. In this connection, recent calculations have indicated very favorable results with low molecular weight gases (secondary flow) such as helium.

SECTION VI

REFERENCES

1. McArdle, Jack G. Internal Characteristics and Performance of an Aerodynamically Controlled, Variable Discharge Convergent Nozzle. NACA TN 4312, July 1958.

2. Lingen, A. Jet-Induced Thrust-Vector Control Applied to Nozzles Having Large Expansion Ratios. Research Report No. R-0937-33, United Aircraft Corporation, March 1, 1957.

3. Martin, A. I. The Aerodynamic Variable Nozzle. Journal of the Aeronautical Sciences, Vol. 24, No. 5, p. 357, May 1957.

4. Equations, Tables, and Charts for Compressible Flow by the Ames Research Staff, NACA TR 1135, 1953.

5. Ippen, A. T., and Harleman, D. R. F. Studies on the Validity of the Hydraulic Analogy to Supersonic Flow. WADC Technical Report No. 5895, Parts I and II, May 1950.

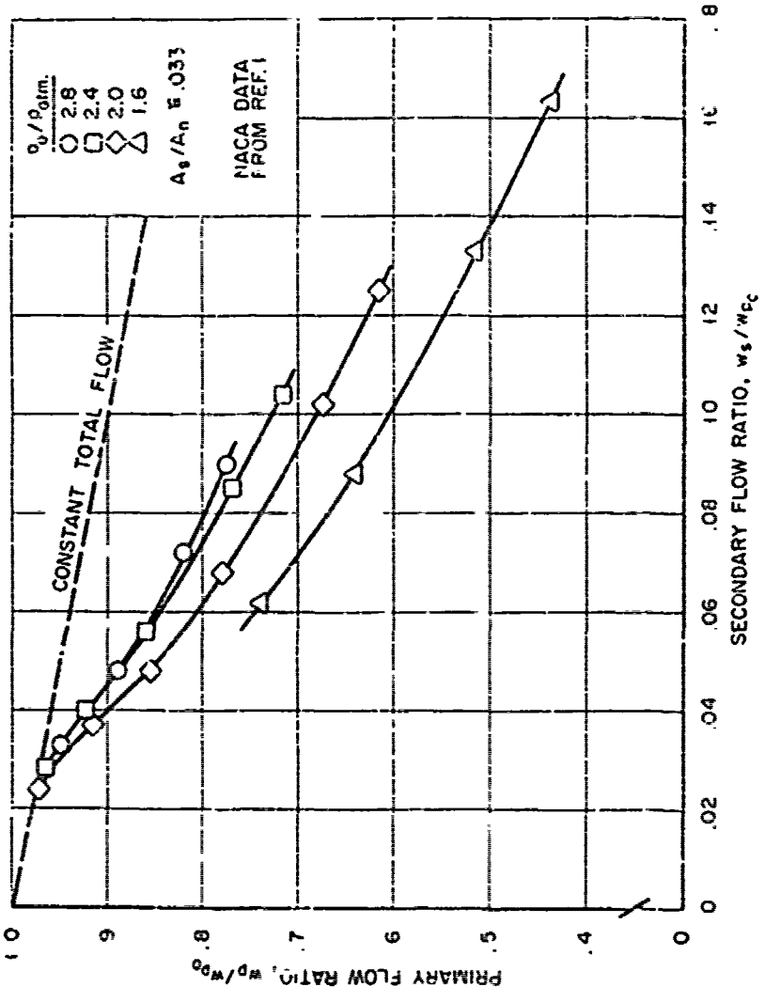

Figure 1. Effect of Primary Pressure Ratio (p_o/p_{atm}) on Flow Throttling (NACA Data)

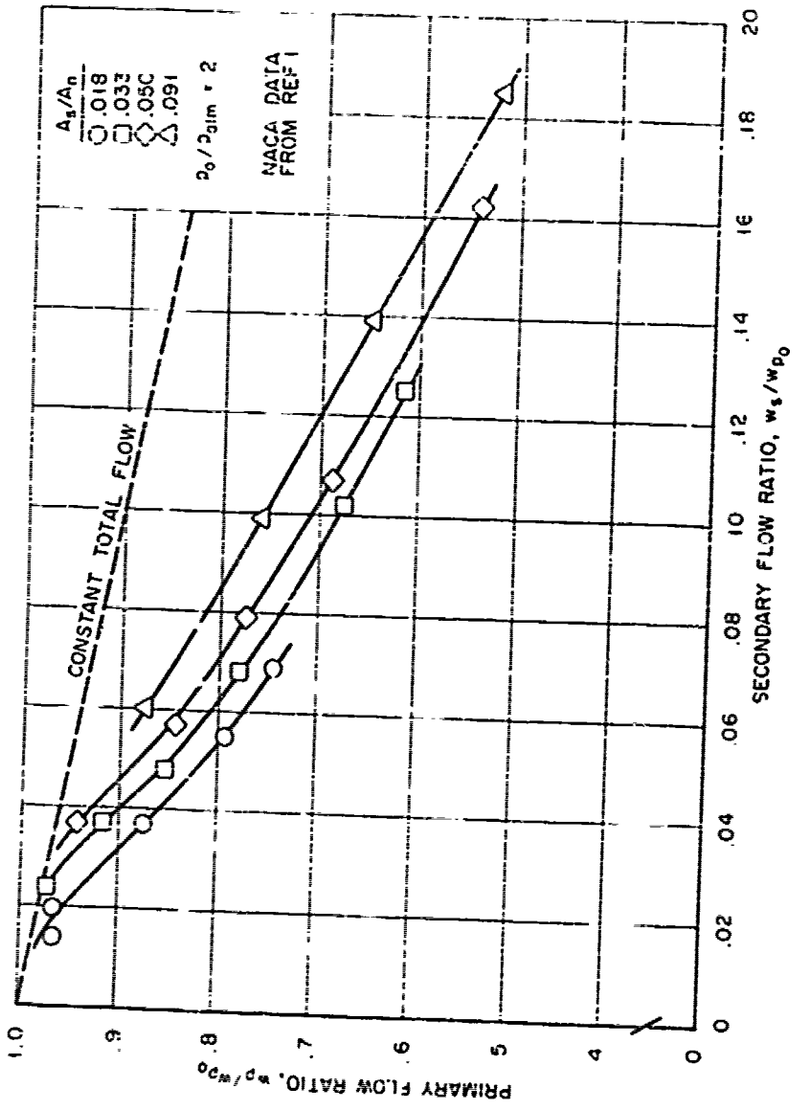

Figure 3. Effect of Injection Slot Width on Flow Throttling (NACA Data)

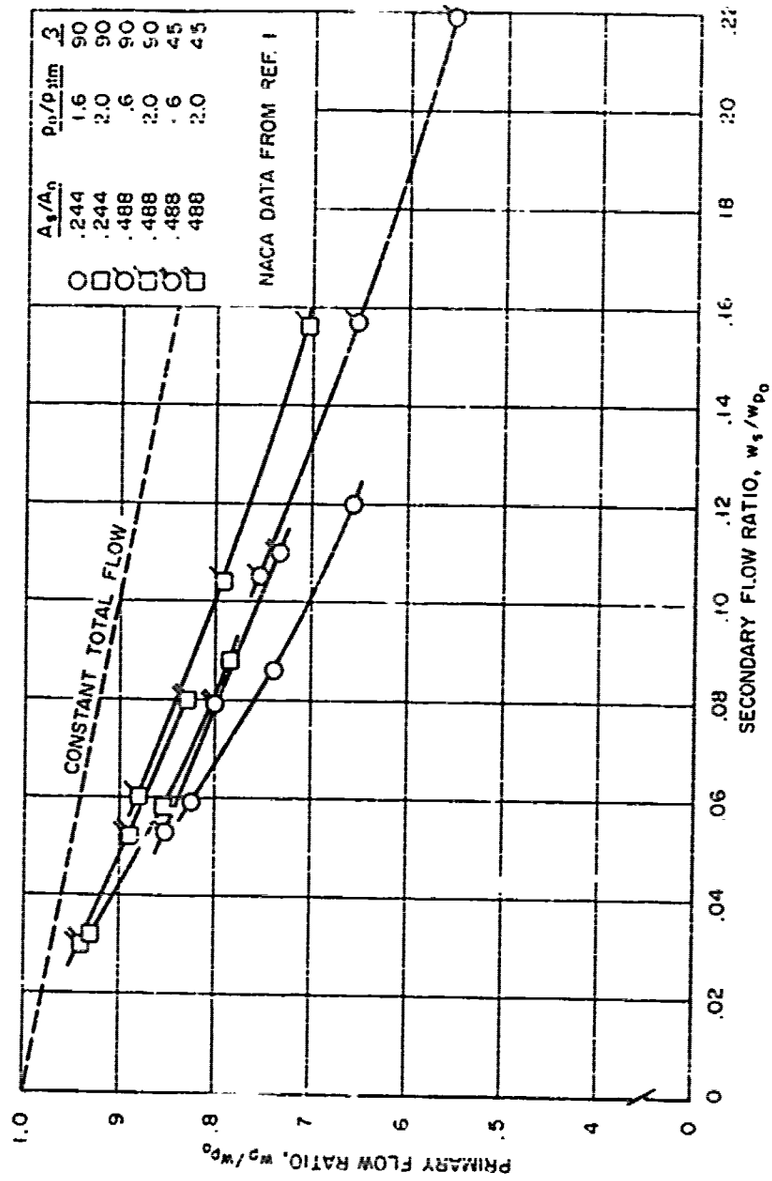

Figure 3. Influence of Primary Pressure Ratio (p_o/p_{atm}), Injection Slot Width, and Circumferential Angle of Injection (β) on Side Force (NACA Data)

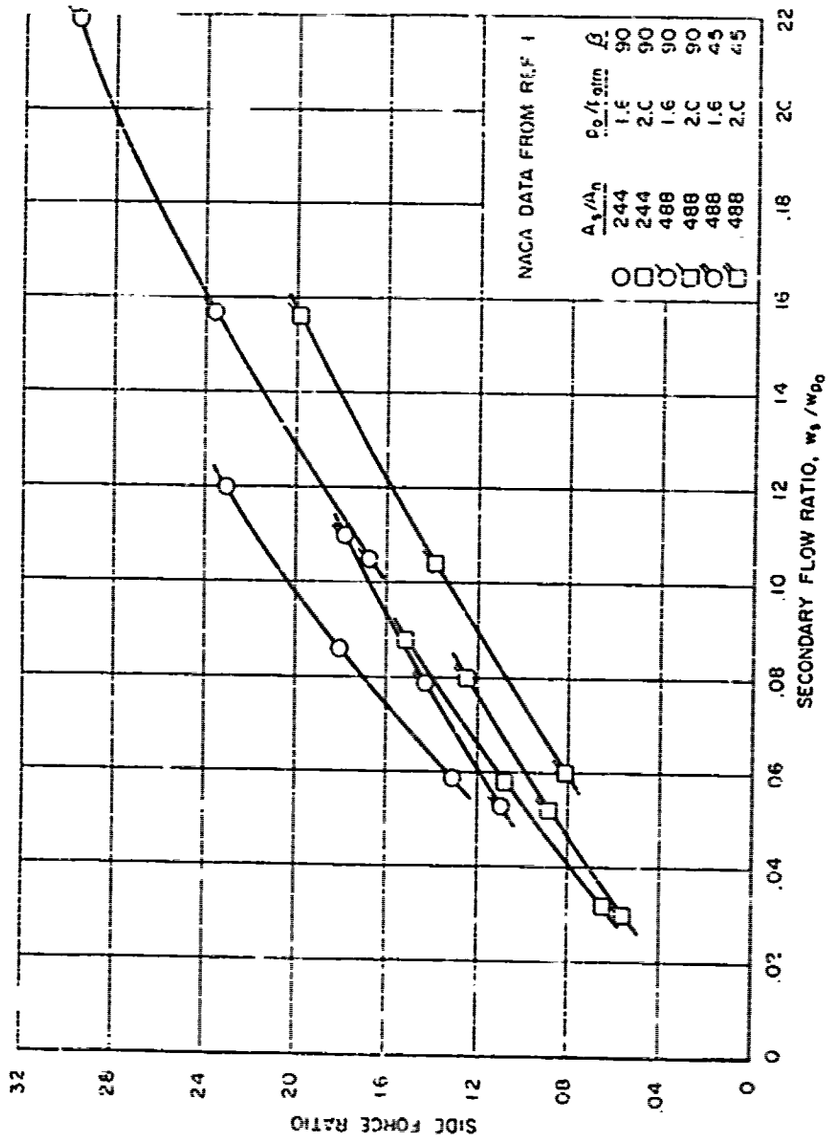

Figure 4. Influence of Primary Pressure Ratio (p_o/p_{atm}), Injection Slot Width, and Circumferential Angle of Injection (β) on Side Force (NACA Data)

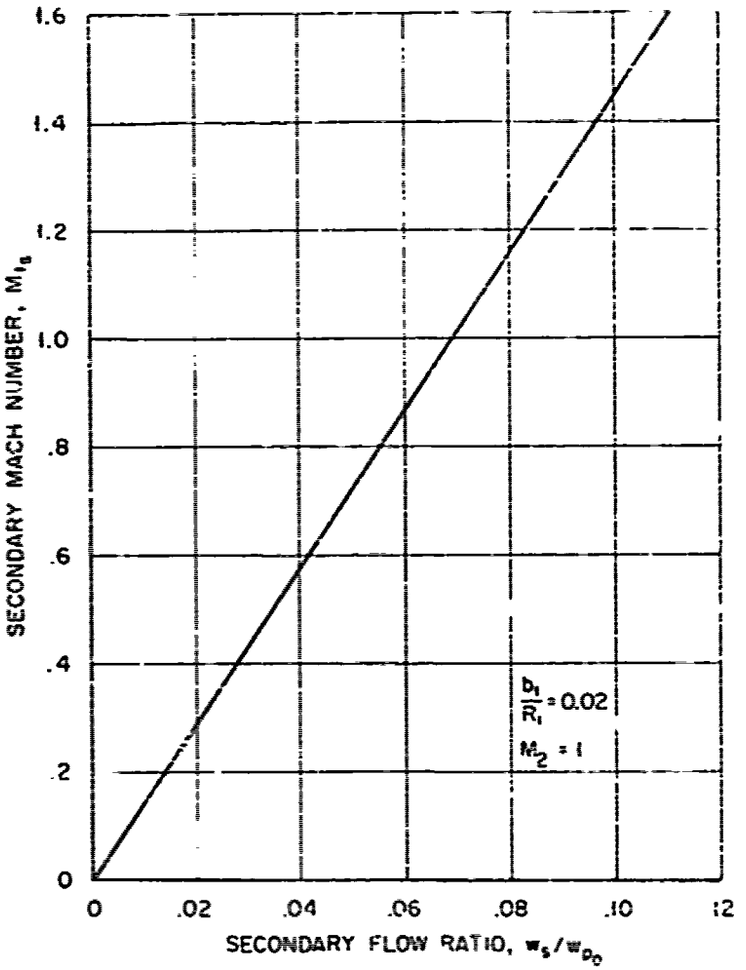

Figure 5. Variation of Secondary Mach Number M_{1_s} with Secondary Flow Ratio for Martin Theoretical Models

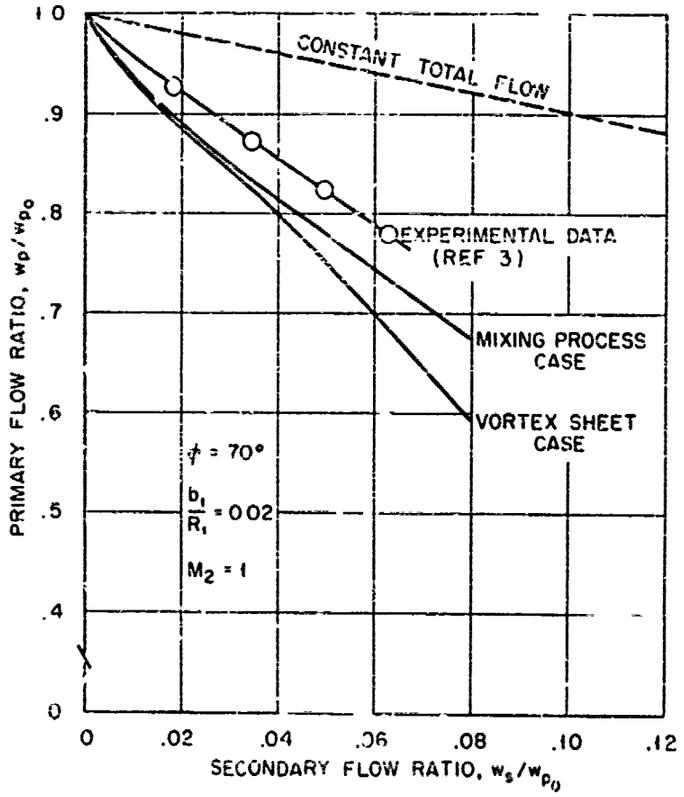

Figure 6. Flow Throttling Results for Martin's Theoretical Models and Experiment (Ref.)

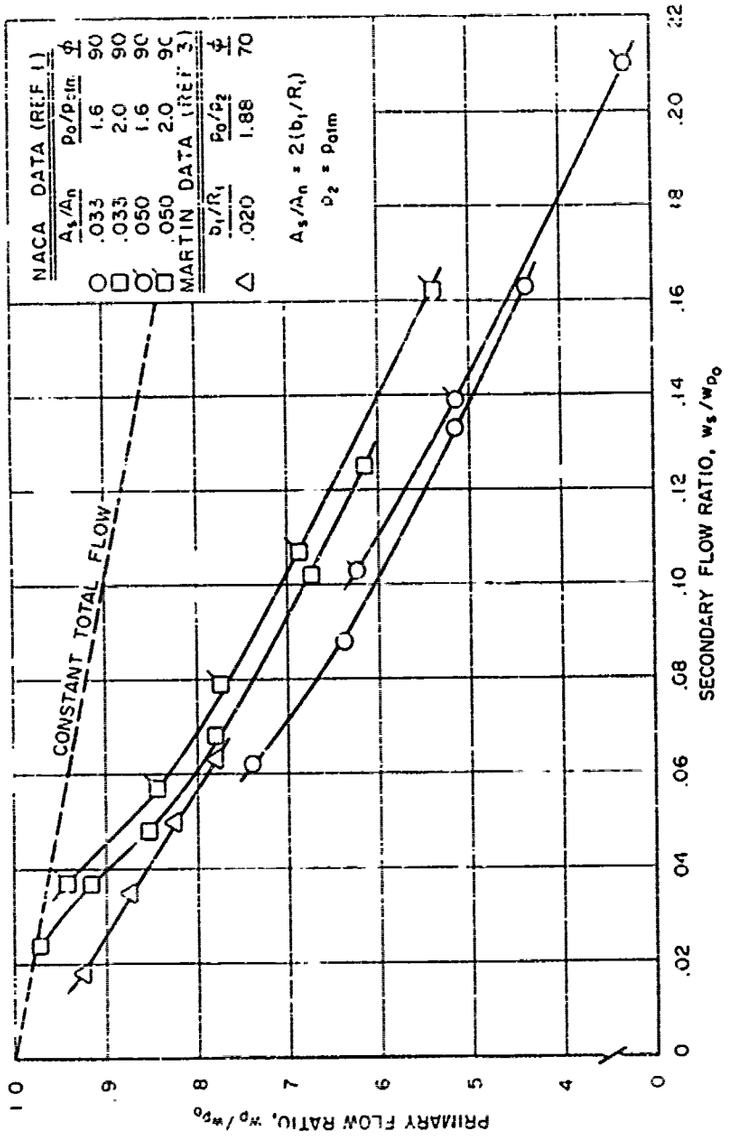

Figure 7. Comparison of NACA (Ref. 1) and Martin (Ref. 3) Flow Throttling Data

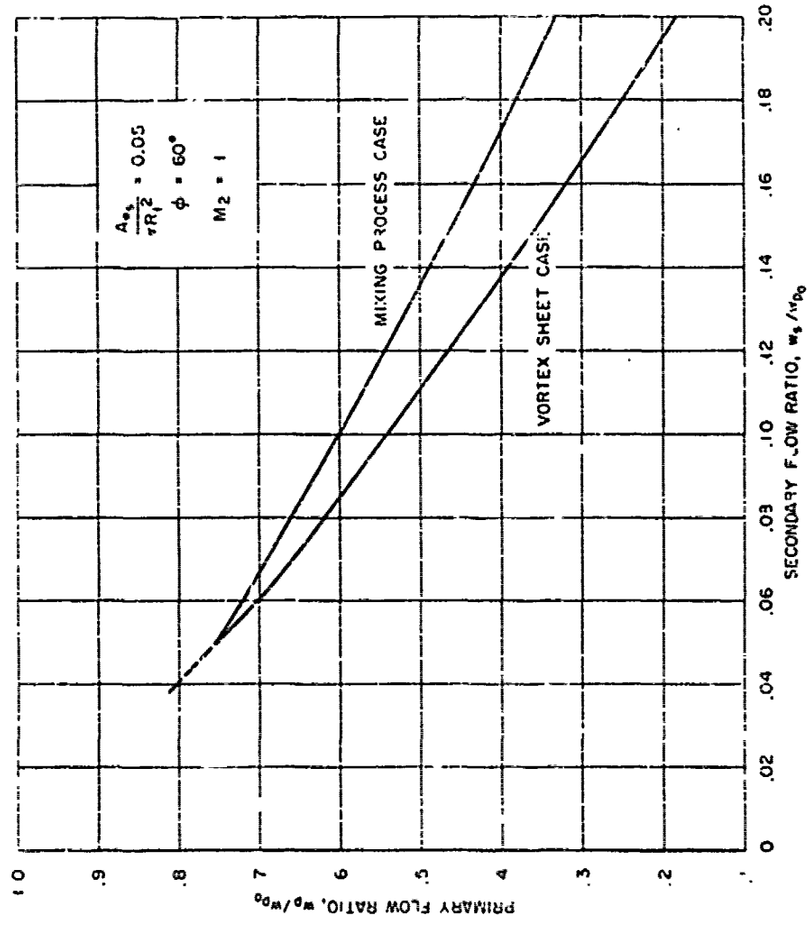

Figure 8. Flow Throttling Results for Modified Martin Theoretical Models

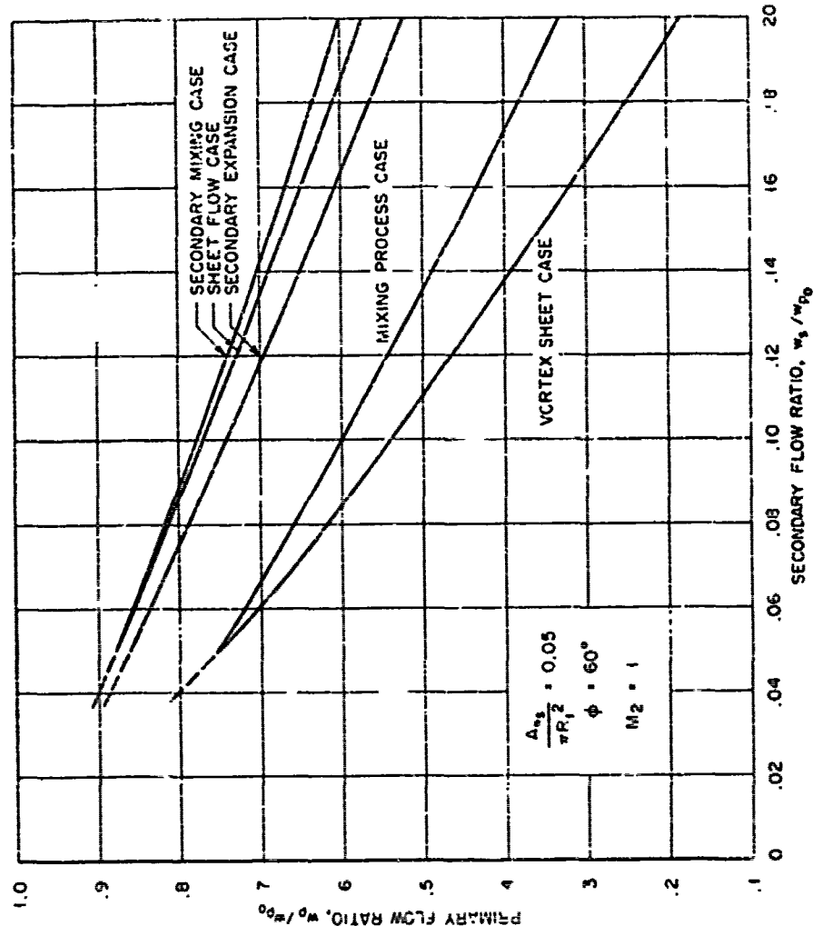

Figure 9. Comparison of Flow Throttling Results for NSL and Modified Martin Models

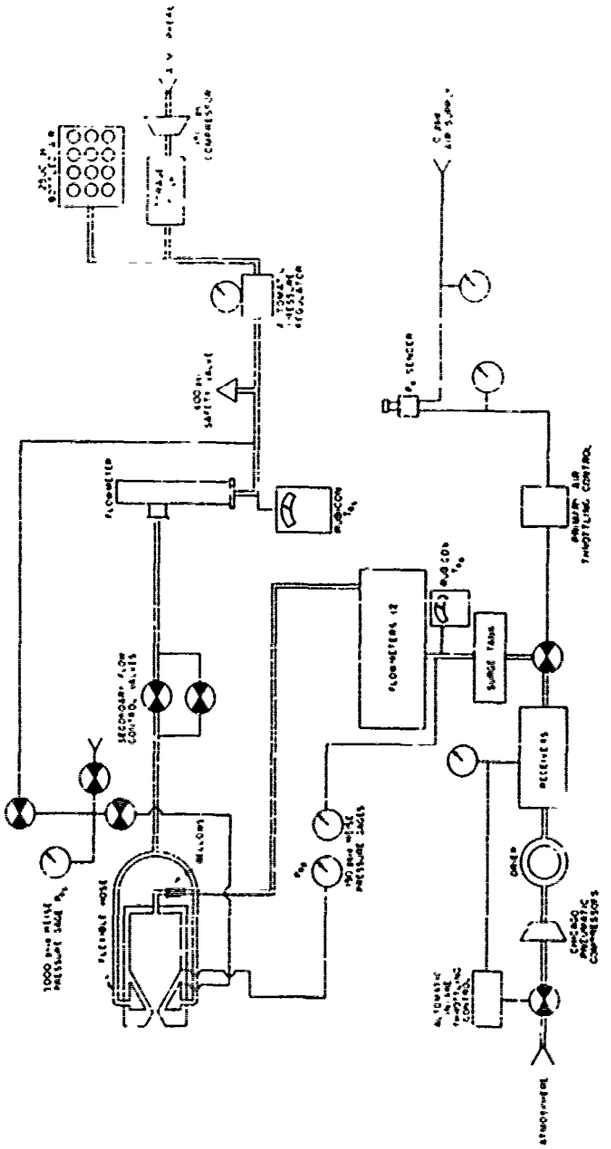

Figure 10. Schematic Diagram of Primary and Secondary Air Supply Systems

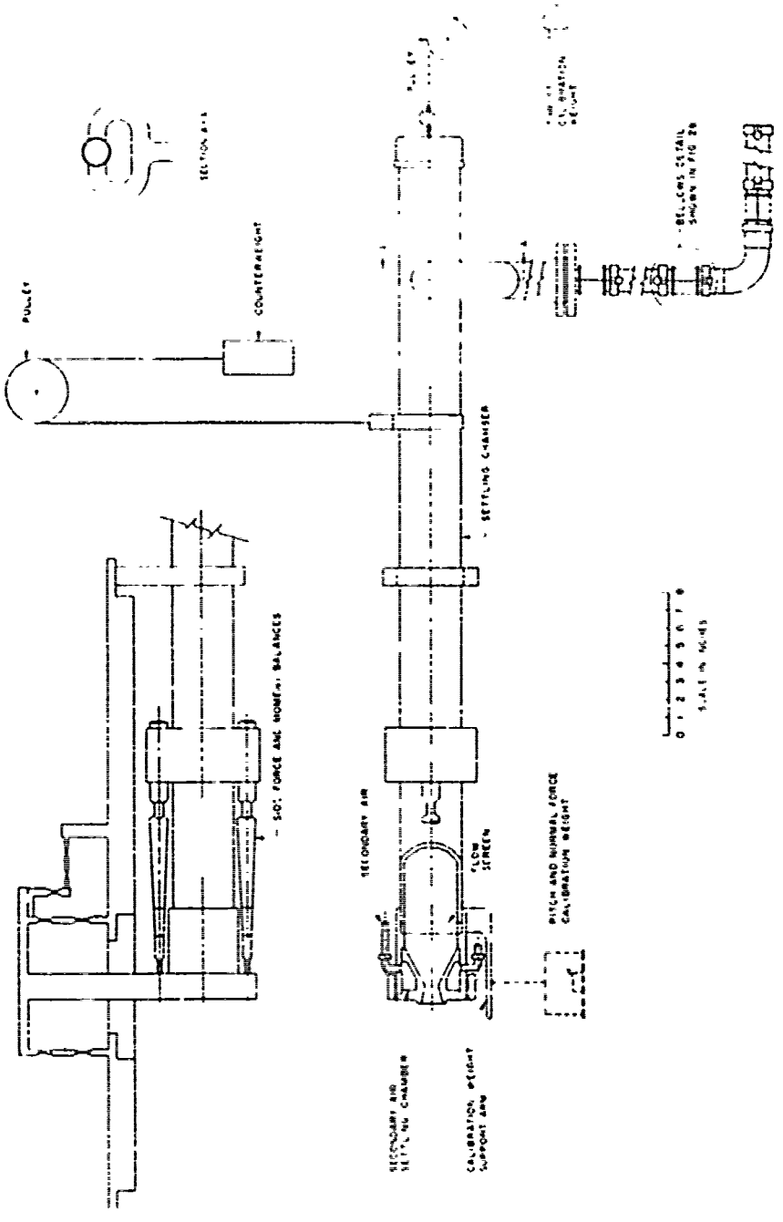

Figure 11a. Model Arrangement

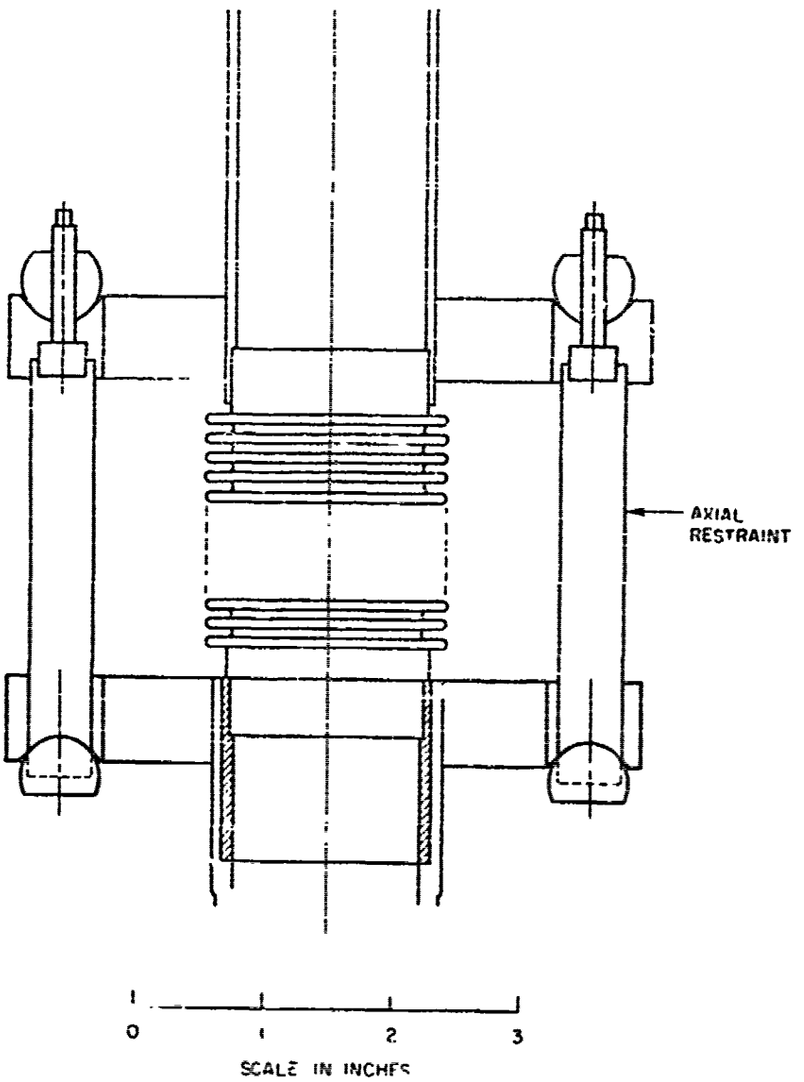

Figure 11b. Bellows Detail

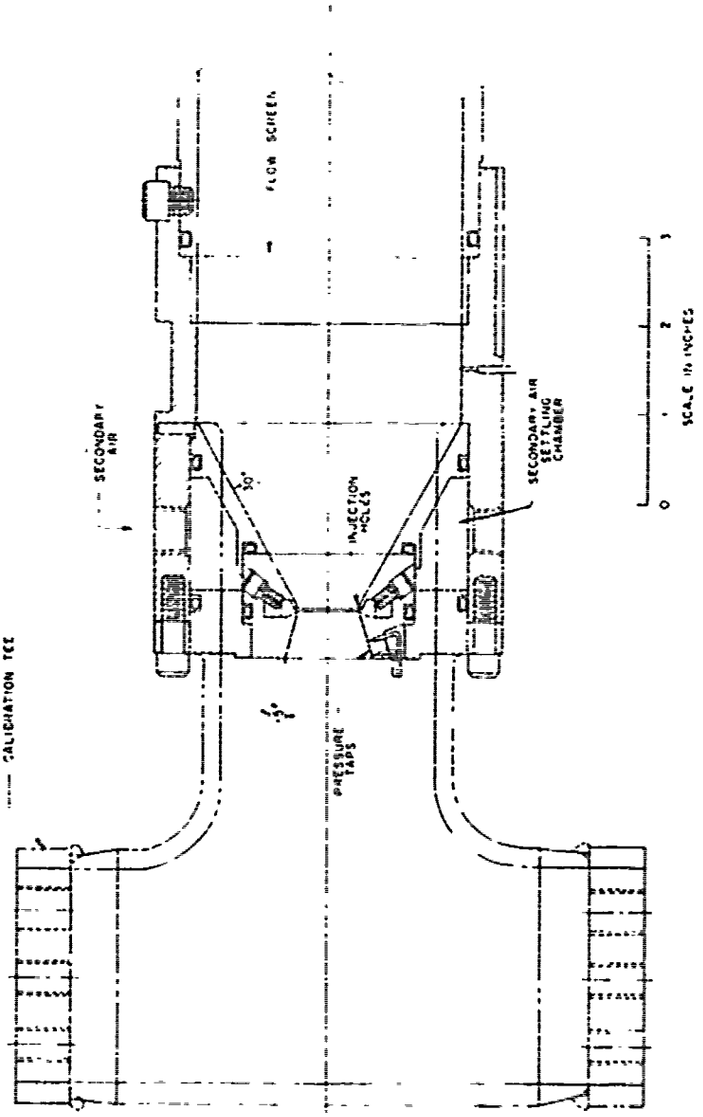

Figure 12. Nozzle Details

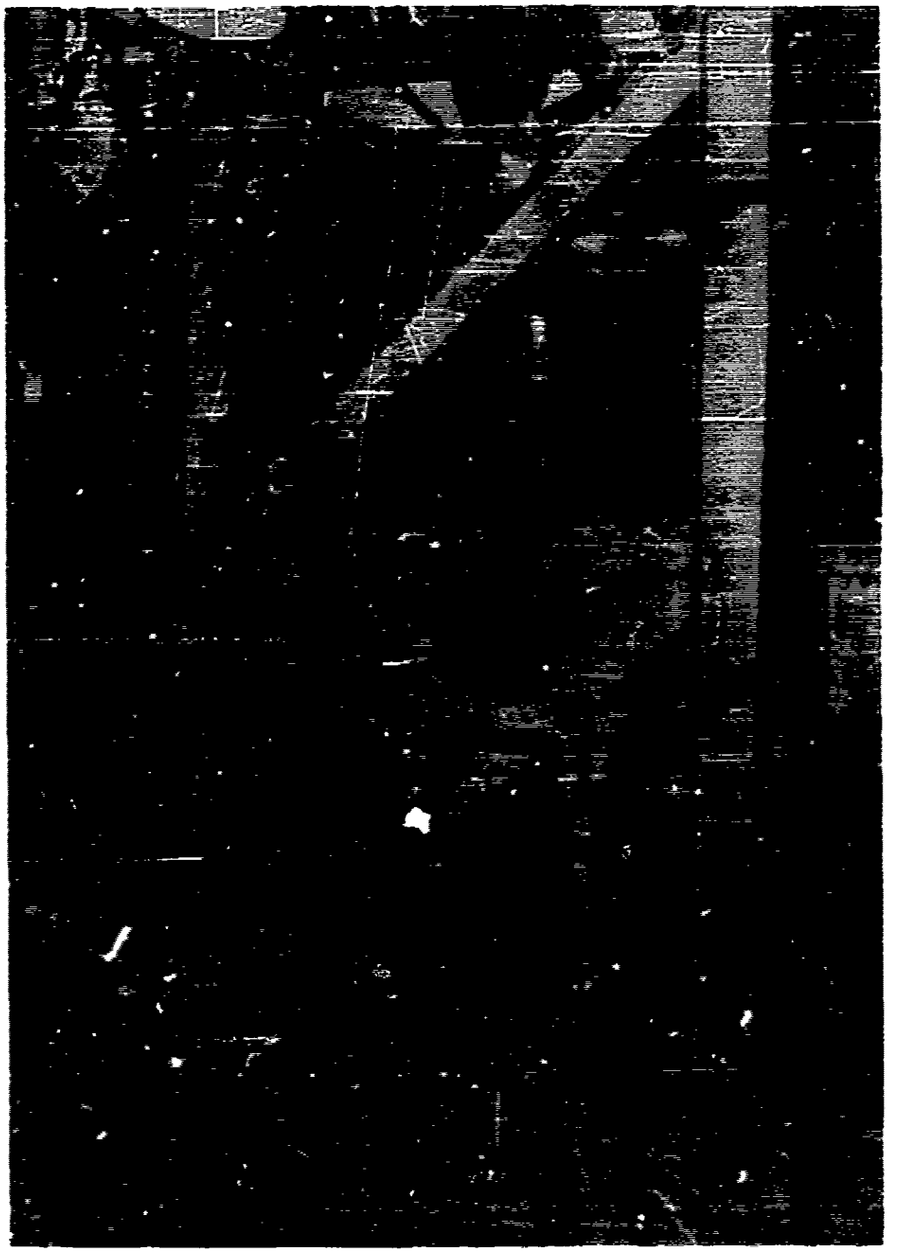

Figure 13. Model installation

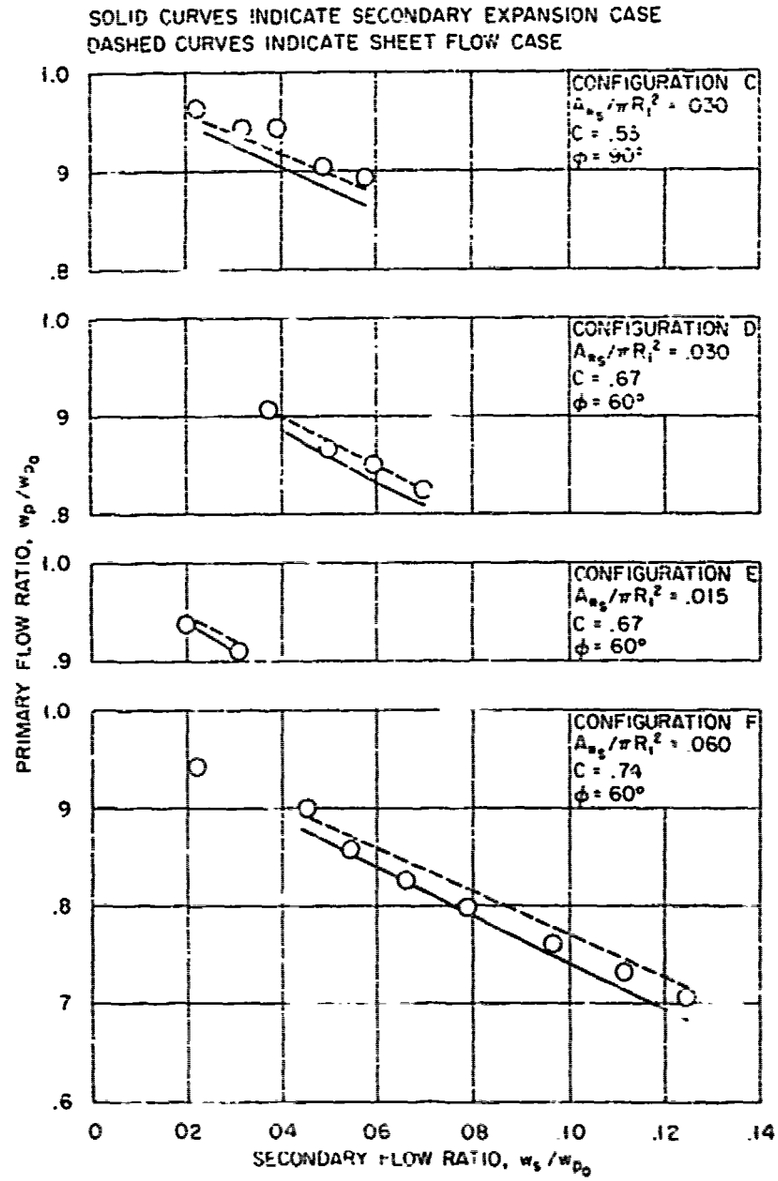

Figure 14. Effect of Injection Angle (ϕ) and Number of Orifices on Flow Throttling

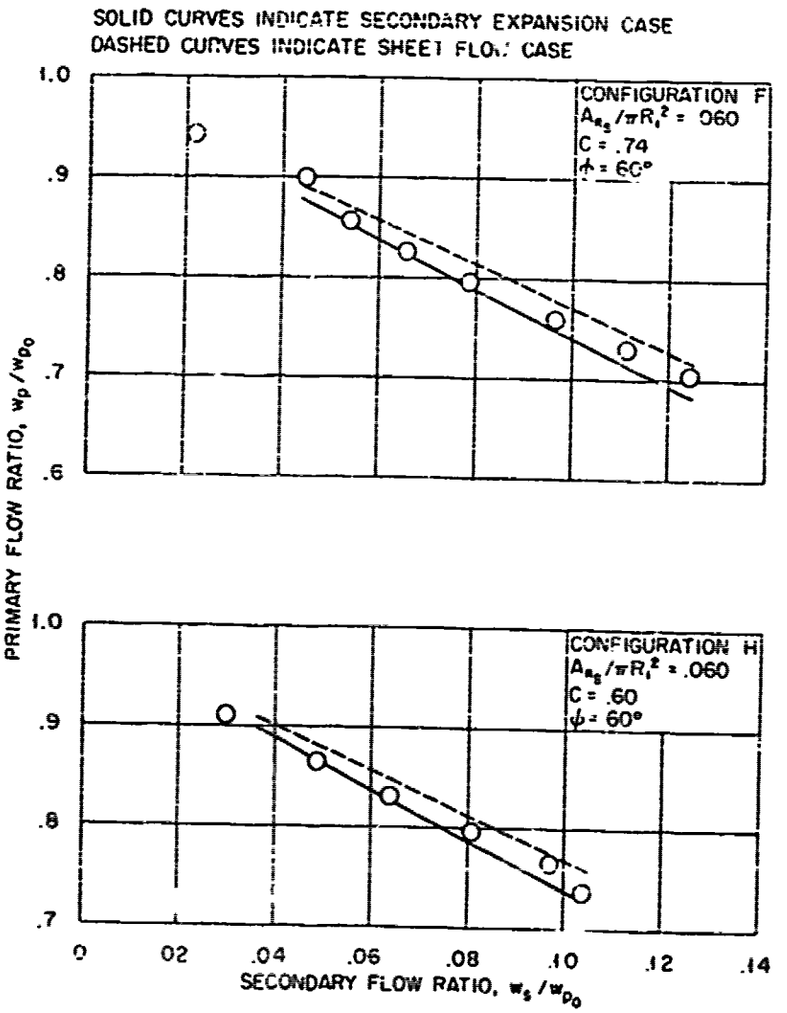

Figure 15. Effect of Slight Variation in Primary Nozzle Contour on Flow Throttling

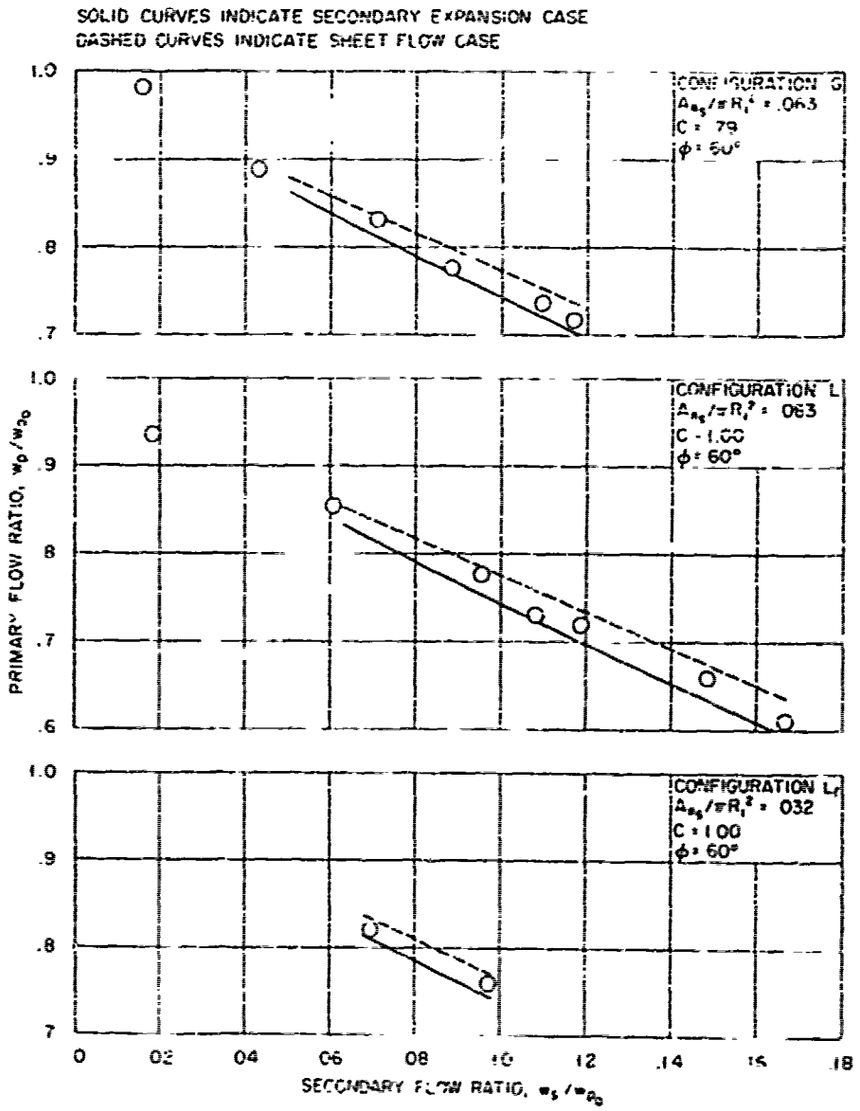

Figure 16. Influence of Number and Shape of Injection Orifices on Flow Throttling

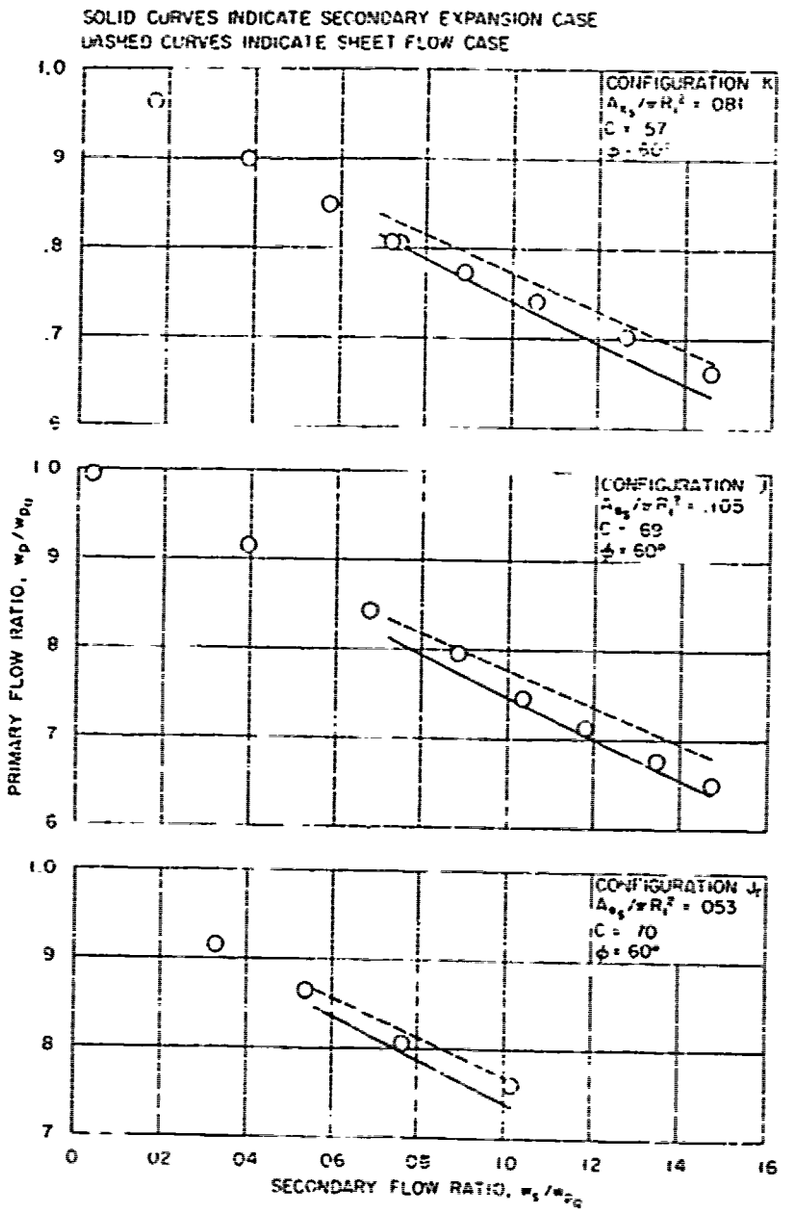

Figure 17 Comparison of Orifice, Slot, and Injection Flow Throttling Performance

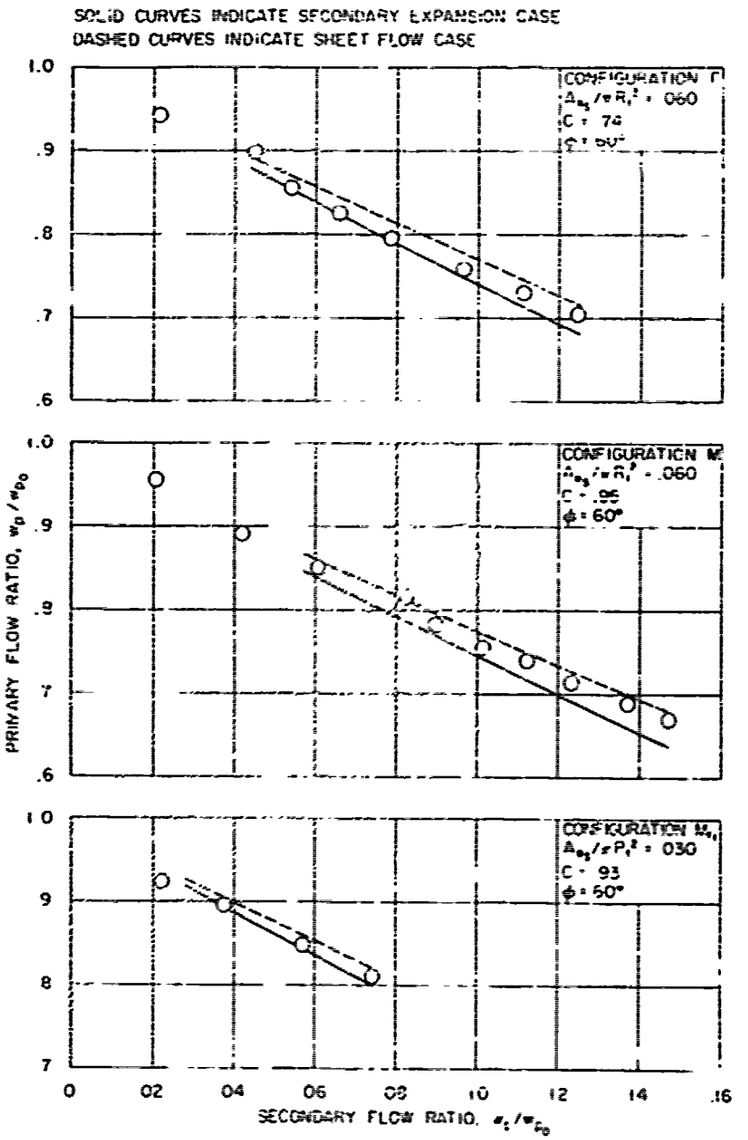

Figure 18. Effect of Nozzle Contour and Number of Injection Orifices on Flow Throttling

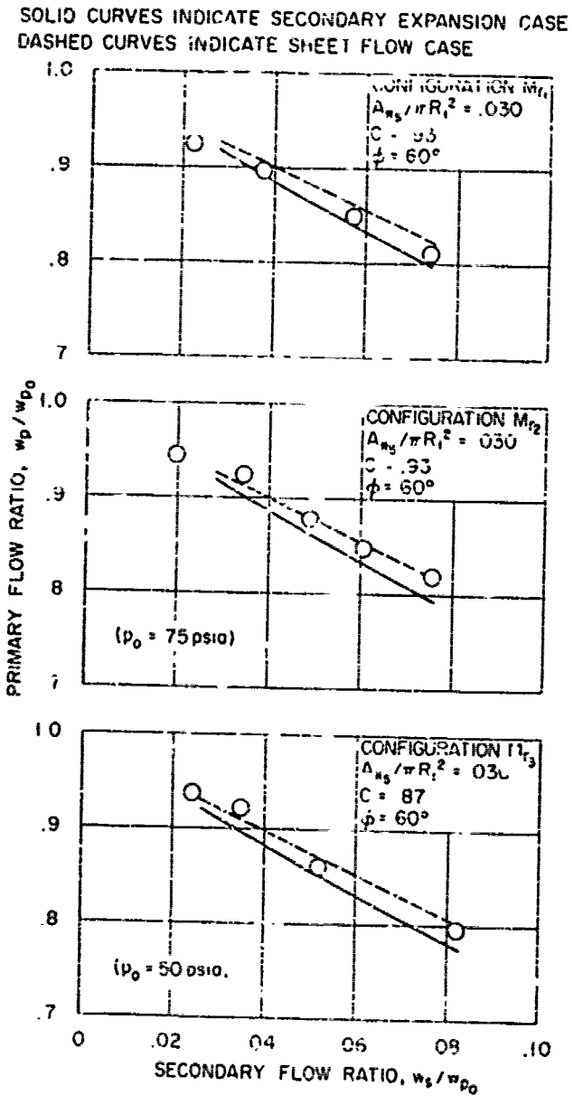

Figure 19. Influence of Primary Pressure Ratio on Flow Throttling

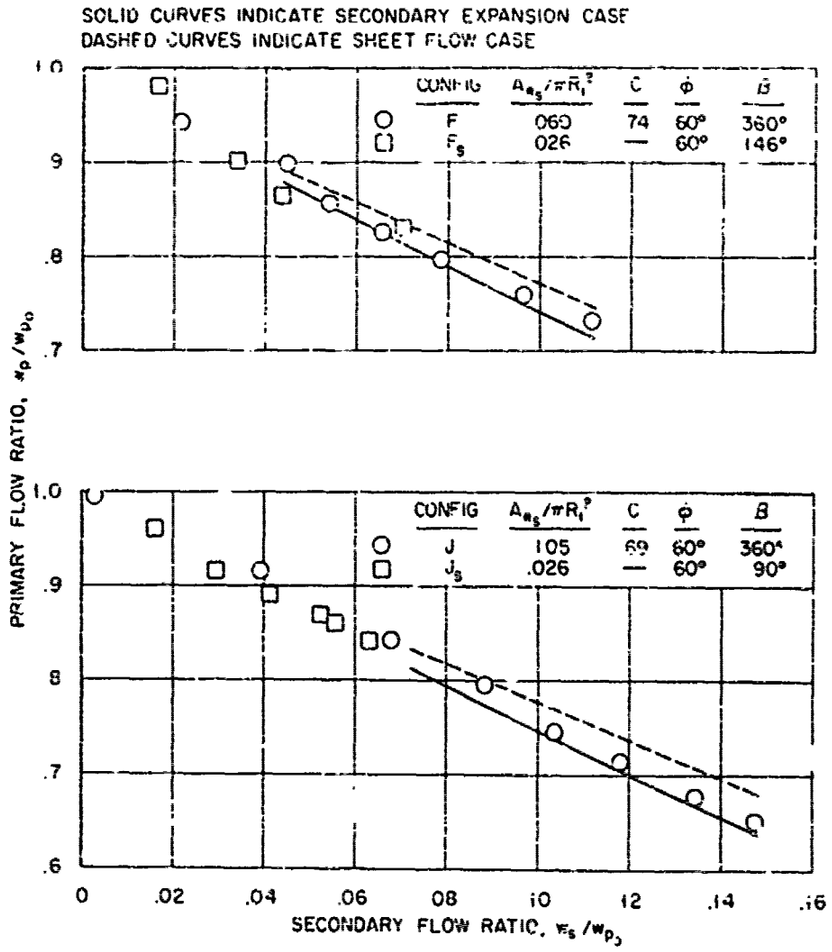

Figure 22. Comparison of Symmetric and Asymmetric Injection Flow Throttling

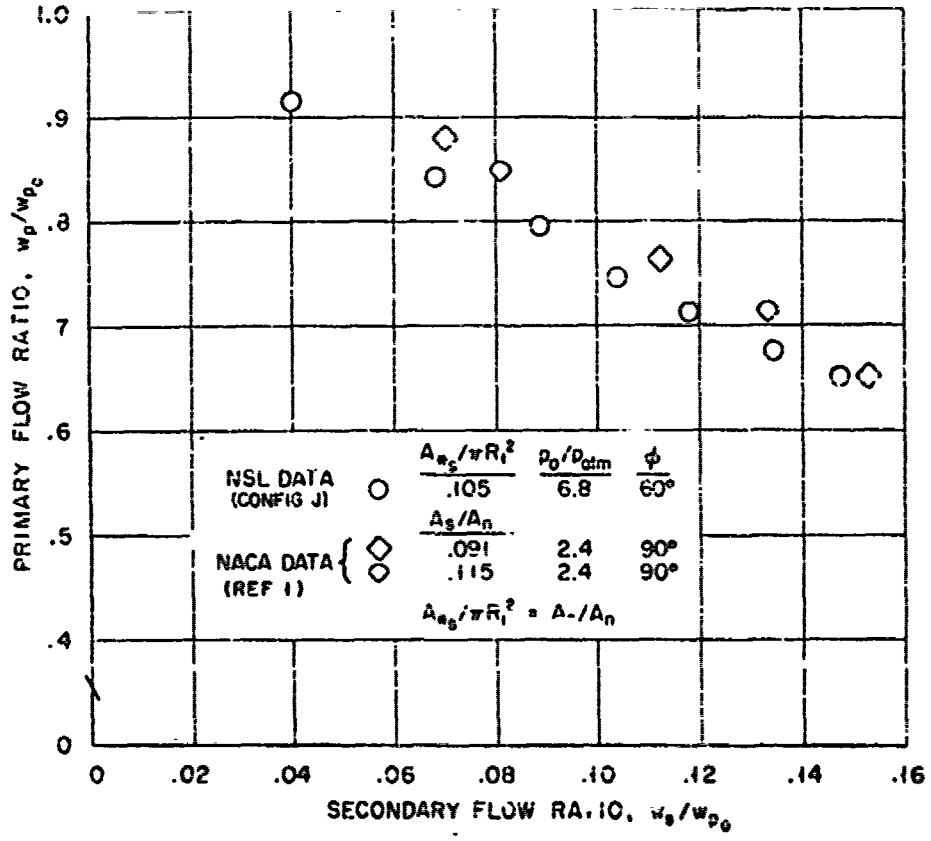

Figure 21. Comparison of NSL and NACA Flow Throttling Data

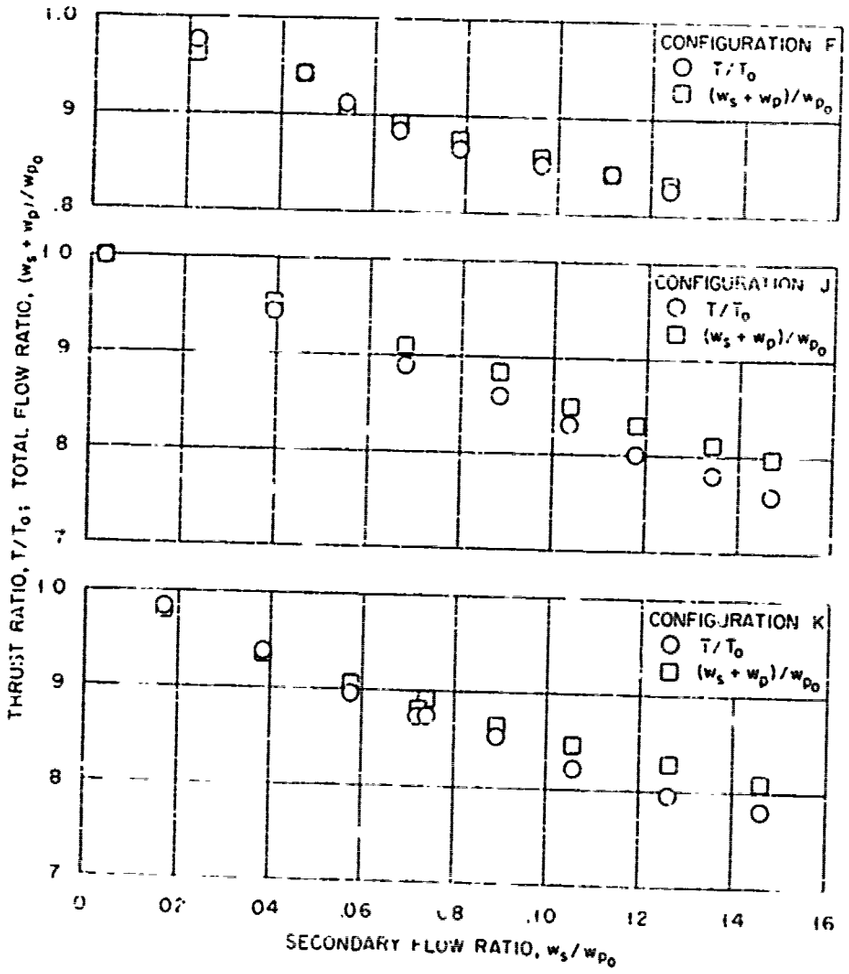

Figure 32. Variation of Thrust and Total Nozzle Flow with Secondary Flow

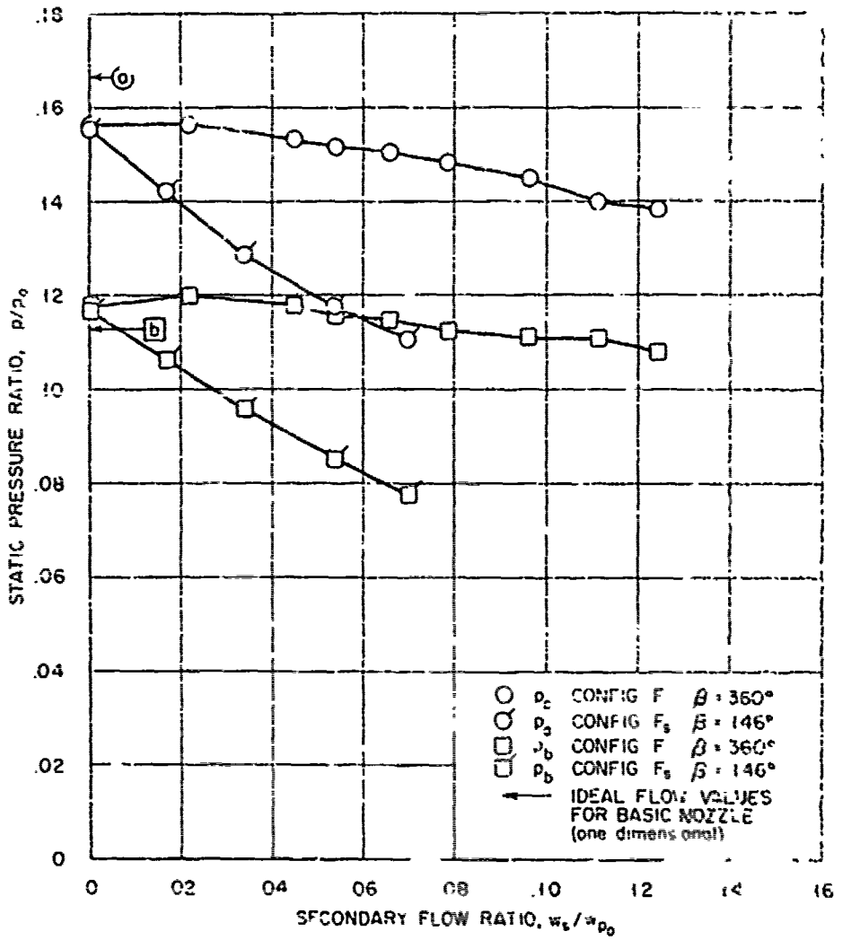

Figure 7. Influence of Symmetric and Asymmetric Injection of Nozzle Pressure at Two Stations